Palaeogeography, Palaeoclimatology, Palaeoecology 659 (2025) 112663

Contents lists available at ScienceDirect

Palaeogeography, Palaeoclimatology, Palaeoecology

journal homepage: www.elsevier.com/locate/palaeo

Integrating high-resolution Sr/Ca and ultrastructural analyses of the *Tridacna squamosa* shell to reconstruct sub-daily seawater temperature variation

Cornélia Brosset [a,*], Chengcheng Liu [b], Haotian Yang [b], Hong Yan [b,*], Bernd R. Schöne [a,*]

[a] Institute of Geosciences, University of Mainz, Joh.-J.-Becher-Weg 21, 55128 Mainz, Germany
[b] State Key Laboratory of Loess and Quaternary Geology, Institute of Earth Environment, Chinese Academy of Sciences, Xi'an 710061, China

ARTICLE INFO

Editor: Prof. M Elliot

Keywords:
Bivalve sclerochronology
Biological clock
Discretized Sr/Ca analysis
Ultrastructure-specific chemistry
Sub-daily temperature

ABSTRACT

Modern and fossil bivalves record environmental variability in their shells in the form of chemical and ultrastructural properties as well as changes in growth rate. These proxy data can be placed in precise temporal context based on growth pattern analysis. Some species such as tridacnids grow particularly fast providing unique insights into environmental changes on the time scale of weather which opens new opportunities for paleoclimate research. Here, we assessed the potential use of the fluted giant clam (*Tridacna squamosa*) to reconstruct sub-daily sea surface temperature (SST) fluctuations from shell Sr/Ca ratios. Through a combined µm-scale analysis of shell Sr/Ca (NanoSIMS) and ultrastructure (SEM) it was possible to study shell material produced during daytime (growth increments) and nighttime (growth lines) separately. Unlike coarser resolution chemical analysis (LA-ICP-MS and ICP-OES), this approach revealed a significant positive correlation between SST and Sr/Ca during daytime ($R^2 = 0.36$, $p < 0.001$). The correlation further increased when the NanoSIMS data of several consecutive daily increments were combined to match the sampling resolution of LA-ICP-MS and ICP-OES data, i.e., four days to two weeks (R^2 of up to 0.86, $p < 0.001$). With an uncertainty of at least ± 1.5 °C, the applicability of the Sr/Ca thermometer remains limited considering that *T. squamosa* only occurs in ecosystems with minimal seasonal temperature amplitudes. Consistent daily Sr/Ca cycles were observed with local maxima at growth lines. This cyclic pattern was found even when the ultrastructure morphology varied or when the complex crossed-lamellar ultrastructure of the shell deviated from its typical configuration during extreme weather events. Therefore, Sr/Ca is likely not directly linked to the shell ultrastructure, but instead both properties are driven by underlying physiological factors.

1. Introduction

Bivalves record environmental variability in their shells in the form of chemical and structural properties (Peharda et al., 2021). These data can be accurately aligned in time by means of growth pattern analysis, specifically if the date of death is known (Jones, 1981; Fritz and Haven, 1983; Chauvaud et al., 1998; Clark, 2005). Shells of long-lived, slow-growing species can provide unique insights into the climatic history of aquatic ecosystems and inform about environmental changes on time-scales of decades to centuries and possibly beyond (Jones, 1980, 1981; Weidman et al., 1994; Marchitto et al., 2000; Schöne et al., 2005, 2020; Butler et al., 2013; Reynolds et al., 2016; Tanabe et al., 2017). Environmental data on the time-scale of seasons and weather, on the other hand, can be obtained from either shorter-lived species (Carré et al., 2013; Jolivet et al., 2015; Füllenbach et al., 2015) or juvenile shell portions of long-lived bivalves (Yan et al., 2013, 2015, 2020), because both grow rapidly enough to enable the reconstruction of changes on time-scales of days or even hours.

Tridacnids, also known as giant clams, belong to the latter category. They inhabit shallow waters in the sub/tropical Indo-Pacific since ca. 55 million years (Rosewater, 1965). These bivalves are renowned for their long lifespan (up to 100 years) (Rosewater, 1965), large size (of up to 1 m in length) (Rosewater, 1965) and rapid biomineralization during youth with growth rates of several cm per year (Lucas et al., 1989; Van Wynsberge et al., 2017). During the first years of life, they lay down distinct daily growth bands (Aharon and Chappell, 1986; Pätzold et al.,

* Corresponding authors.
E-mail addresses: cornelia.brosset@uni-mainz.de (C. Brosset), yanhong@ieecas.cn (H. Yan), bernd.schoene@uni-mainz.de (B.R. Schöne).

https://doi.org/10.1016/j.palaeo.2024.112663
Received 26 June 2024; Received in revised form 4 October 2024; Accepted 6 December 2024
Available online 8 December 2024

1991; Watanabe and Oba, 1999; Hori et al., 2015; Yan, 2020; Arndt et al., 2023) consisting of couplets of a growth line (formed during the night) and a growth increment (formed during the day). Due to their autofluorescence, the daily growth lines can be studied most effectively by means of Laser Scanning Confocal Microscopy (LSCM) (Liu et al., 2022) and provide a means to date each shell portion to the nearest day. As in other bivalve species, the most critical and hotly debated aspect is how specific environmental variables can be quantitatively reconstructed from the shells (Peharda et al., 2021), in particular the most relevant climate parameter, water temperature. While this is traditionally accomplished with shell oxygen isotope ($\delta^{18}O$) values (Epstein et al., 1953; Mook and Vogel, 1968; Aharon, 1983; Watanabe and Oba, 1999), in settings with seasonally fluctuating $\delta^{18}O_{water}$ values (and salinity to which $\delta^{18}O_{water}$ is linearly correlated), it would be advantageous to verify temperature estimates with another proxy or use both in combination to infer past temperature and salinity data. Shell Sr/Ca has made it on the shortlist, because this ratio works well in many scleractinian corals (Beck et al., 1992; Corrège, 2006) and abiogenic aragonite (Gaetani and Cohen, 2006). In addition, Sr/Ca_{water} (other than $\delta^{18}O_{water}$) is considered relatively stable above a salinity of 10 (Dodd and Crisp, 1982) and can thus be neglected in respective paleothermometry equations. However, in bivalves including tridacnids the use of Sr/Ca as a temperature indicator is controversially debated. While in some studies a negative correlation between shell Sr/Ca of giant clams and the seasonal temperature variation was reported (Sano et al., 2012; Yan et al., 2013; Liu et al., 2021), other authors found the opposite (Arias-Ruiz et al., 2017; Liu et al., 2021). As tridacnids host photosymbionts in their tissue which supply the bivalve with energy to regulate physiological processes (Bonham, 1965; Rosewater, 1965; Klumpp and Lucas, 1994; Griffiths and Klumpp, 1996), shell Sr/Ca fluctuations on both daily and seasonal time-scales have been linked to photosynthetic efficiency and insolation (Sano et al., 2012). Still others explained the diurnal Sr/Ca changes by physiological processes related to circadian biological rhythms (Warter et al., 2018).

Physiological processes not only influence the shell element chemical content (Lorens and Bender, 1977; Ballesta-Artero et al., 2017; Barrat et al., 2023), but also ultrastructural patterns (Ballesta-Artero et al., 2017; Höche et al., 2022). As a result, a mathematical correlation may be found between these two properties (Lazareth et al., 2013; DeWinter et al., 2021; Brosset et al., 2022, 2023). For example, higher Sr concentrations are typically measured in growth lines (reflecting times of reduced shell growth) rather than growth increments (reflecting periods of fast growth and thus the main growing portion of each day) (Foster et al., 2009; Schöne et al., 2011, 2013; Shirai et al., 2014; Füllenbach et al., 2017). The former often consists of irregular simple/spherulitic prismatic ultrastructure, whereas the latter is ultrastructurally more complex (Schöne et al., 2013). In tridacnids, shell Sr/Ca profiles also exhibit local peaks at daily growth lines (Sano et al., 2012; Warter and Müller, 2017; Warter et al., 2018; Yan et al., 2020), which likewise consist of irregular prisms. Lower Sr/Ca values, however, are observed in the daily growth increments, which are primarily composed of a complex crossed-lamellar (CCL) ultrastructure (Agbaje et al., 2017; Mills et al., 2024a). Such ultrastructural variability supposedly biases temperature reconstructions based on shell Sr/Ca. As demonstrated recently by Brosset et al. (2023), Sr/Ca values of laboratory-grown bivalve shells revealed stronger positive correlations with temperature than such formed in the field. Furthermore, in tridacnid shells, ultrastructural changes correlate with Sr/Ca (Mills et al., 2024b), likely due to environmental stress. Following these authors, shells of *Tridacna squamosa* grown in turbid waters contained CCL ultrastructure covered by prisms (CCL-P configuration). Sr/Ca ratios in CCL-P were lower than in the typical shell ultrastructure (CCL-I configuration, without prisms) formed in clearer waters. Therefore, a detailed understanding of the link between shell strontium content and ultrastructure may be crucial to accurately interpret Sr/Ca data from tridacnid shells.

The goal of the present study was to investigate the variability of shell Sr/Ca ratios in *T. squamosa* in relation to SST fluctuations. High-resolution in-situ analytical techniques (NanoSIMS, LA-ICP-MS) were used to assess links between Sr/Ca and ultrastructure properties, understand the environmental information preserved in shell Sr/Ca ratios and determine the precision of shell Sr/Ca-based seawater temperature estimates. Results of this study can potentially contribute to a more efficient use of shell Sr/Ca to reconstruct past water temperatures in sub/tropical settings.

2. Materials and methods

2.1. Sample collection and preparation

To reconstruct sub-daily SST variations using Sr/Ca ratios from the shell of the fluted giant clam, *T. squamosa*, while accounting for shell architecture variability, high-resolution Sr/Ca and ultrastructural analyses were performed on specimen XB10. It is to be noted that XB10 was misidentified as *Tridacna derasa* in earlier studies (e.g., Yan et al., 2020) and was recently confirmed as *T. squamosa* (Liu et al., 2024). This specimen was collected from the North Reef (17°05′N, 111°30′E) in the northern South China Sea on 9 December 2013. After removal of the soft tissues, one valve was sectioned (Fig. 1A) using a diamond-coated saw blade attached to a cutting machine (for details see Yan et al., 2020). The radial growth portion of the shell slab (Fig. 1B) was embedded in epoxy resin and polished using a fine diamond grain sheet followed by a 0.5 μm diamond suspension. Images of the polished shell section were obtained using a Nikon A1 LSCM (State Key Laboratory for Manufacturing Systems Engineering, Xi'an Jiatong University; Fig. 1D). Triggering the auto-fluorescence of the shell material revealed daily growth lines in the shell (Yan et al., 2020; Fig. 1D).

2.2. Element chemistry and ultrastructure analyses

Shell Sr/Ca data were obtained from specimen XB10 using a CAMECA NanoSIMS 50L (CAMECA, Paris, France), as detailed in Yan et al. (2020). Briefly, the shell was sampled using a Cs^+ beam of approx. 150 pA, 16 kV and approx. 300 nm of diameter after carbon coating of the surface. 25 blocks of 10 cycles were measured by scanning the primary beam across areas of 2 μm^2 for a total of approx. 200 s of integration time and 2 μm spot-by-spot interval. The multi-collector system (mass resolving power of approx. 6000; 10 % definition) enabled the simultaneous measurements of $^{40}Ca^{16}O$ and $^{88}Sr^{16}O$, which were used to obtain semi-quantitative Sr/Ca values in counts/counts. For this study, the data from 15 July 2012 to 3 March 2013 were selected (approx. 4.5 mm representing 7 months of shell growth) as the shell growth lines from this portion were particularly distinctly developed, sharper and clearly separated by growth increments in LSCM images (Fig. 1D).

Lower resolution quantitative shell Sr/Ca data (mmol/mol) were used for comparison with sub-daily Sr/Ca data obtained by NanoSIMS. Yan et al. (2020) reported Sr/Ca data obtained via inductively coupled plasma – optical emission spectroscopy (ICP-OES). Low-resolution Sr/Ca data, reported by Liu et al. (2024), were also measured by laser ablation – ICP – mass spectrometry (LA-ICP-MS).

After element chemical analysis, the shell portion was ground using F800 and F1200 SiC suspensions on glass plates and polished using a 1 μm Al_2O_3 suspension on a Buehler MasterTex cloth. Following each grinding and polishing step, the sample was ultrasonically rinsed in water. The polished shell portion was immersed for 30 min in a 3 vol% H_2O_2 solution to remove organic material from the surface layer (i.e., surface oxidation) of the individual biomineral units (BMUs) of the shell complex crossed-lamellar ultrastructure, facilitating their visualization. The section was then mounted on a one-inch sample holder using a carbon sticker and placed in a Leica EM ACE200 Vacuum Coater for directional sputtering using a 5 nm platinum layer.

To manage the computational load of the SEM analysis and facilitate further image processing, the 4.5 mm long sample was divided into four

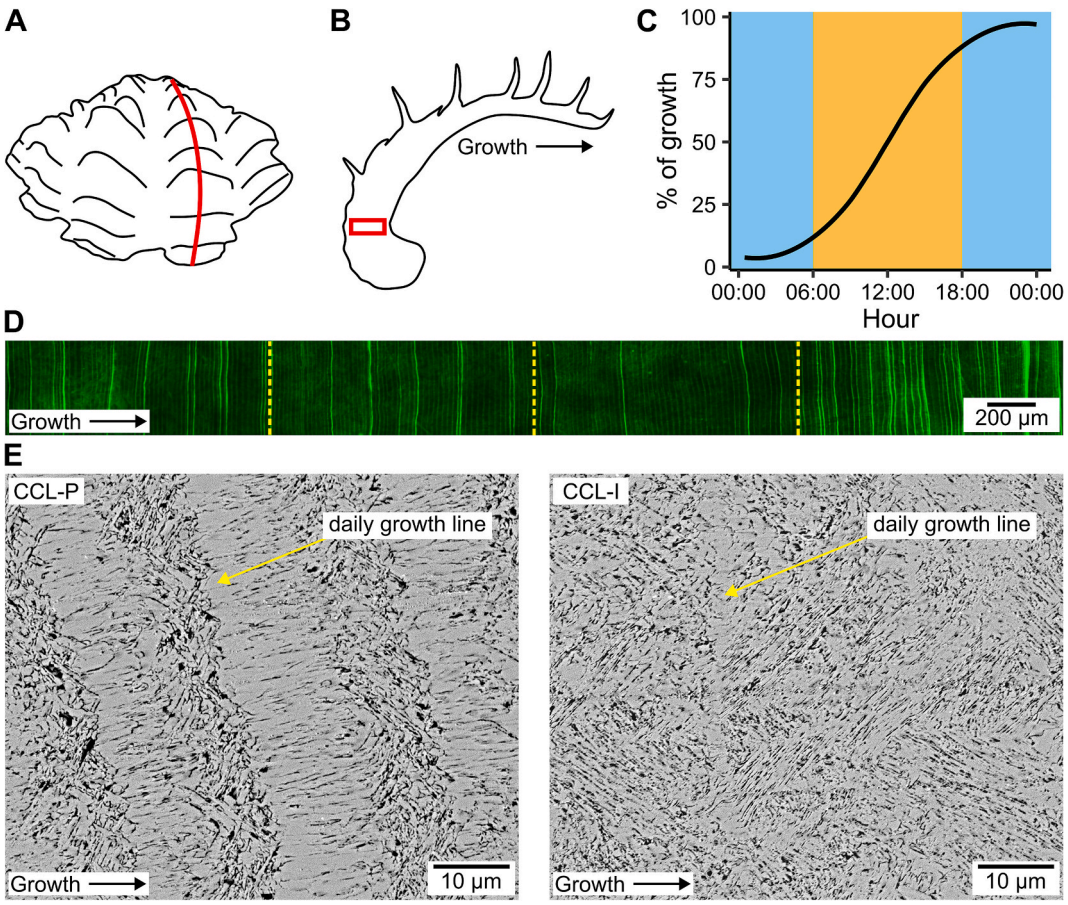

Fig. 1. Overview of sampling and analysis of the studied *Tridacna squamosa* shell. (A) Sketch of the shell. Red line = cutting axis. (B) Schematic cross-section highlighting the area selected for element chemical and ultrastructural analyses (red rectangle). (C) Daily non-linear growth model used for automated temporal alignment of the Sr/Ca and ultrastructural data (size, shape and fractal dimension of the individual biomineral units). Blue and yellow represent data assigned to daily growth lines (formed during night) and increments (formed during day), respectively. (D) Autofluorescence image from Laser Scanning Confocal Microscopy (LSCM) showing the 7-month growth period analyzed in this study, with yellow dashed lines marking the virtual division of the sample into four smaller areas of interest. Daily growth bands are discernable, with growth lines showing higher fluorescence intensity than increments (details in Yan et al., 2020). Note variable LSCM intensity of daily growth lines. (E) Scanning Electron Microscope (SEM) images of the complex crossed-lamellar (CCL) ultrastructure of the shell. The CCL ultrastructure occurs in two configurations, namely complexly intertwined with prisms to the left (CCL-P), and without such prisms to the right (CCL-I). An exemplary daily growth line is indicated by a yellow arrow in each CCL ultrastructure configuration. In panels (B, D, E), the growth direction of the shell is indicated by an arrow. (For interpretation of the references to colour in this figure legend, the reader is referred to the web version of this article.)

smaller areas of interest (Fig. 1D). Results from these regions were later recombined to generate a comprehensive dataset. Using a preliminary low-resolution SEM scan, a shell portion for which the visualization of the BMUs was optimal and representative of the ultrastructural diversity of the sample – including daily growth lines and increments as well as CCL-I and CCL-P configurations – was selected for each area of interest. Each portion had a standard height of approx. 500 µm, ensuring replicability between areas of interest, and was analyzed using automated high-resolution mapping at 5245× magnification performed with a 3rd generation Phenom Pro Desktop SEM, equipped with a backscatter electron detector and a CeB_6 electron source at 10 keV. Individual SEM images were stitched together using the software Fiji/ImageJ (available at https://imagej.net/software/fiji/, last access: 15 April 2024; Schindelin et al., 2012).

2.3. Ultrastructure morphometry

The morphological characteristics of the BMUs (size [area], shape [elongation], complexity [fractal dimension]) were quantified with the Fiji/ImageJ MorphoLibJ plugin (Bogovic et al., 2016; Legland et al., 2016), adapting the methods developed by Höche et al. (2020). To visualize BMU boundaries and remove noise, the contrast of each stitched SEM image was increased and the median grey value subtracted. Images were then converted to binary format, with white representing the BMUs and black the boundaries between them. A watershed transformation algorithm (part of the MorphoLibJ plugin) was used to reconstruct fragmented boundaries. For details see Höche et al. (2020). Once all individual BMUs were labeled with unique identification numbers, the MorphoLibJ plugin was used to determine their size and shape, i.e., the area and elongation.

Each BMU was saved as a region of interest (ROI) using the LabelsToRois plugin (Waisman et al., 2021), allowing for the determination of their fractal dimension using the FracLac plugin (Karperien, 2013) and the box-counting method. For the latter, the number of grid boxes needed to fully cover BMUs is determined. This process is repeated with different grid sizes, and the fractal dimension is determined by analyzing the logarithmic relationship between the number of boxes and the inverse of the box size. For a BMU shape observed in SEM images (2D), the slope of this relationship represents the fractal dimension, which ranges from 1 to 2. A more complex BMU will have a fractal dimension closer to 2, while simpler shapes will have values closer to 1. Thus, the fractal dimension of each BMU in the XB10 shell ultrastructure was calculated as an additional morphometrical parameter indicating complexity and self-similarity.

2.4. Sub-daily temporal alignment of the data

In previous research, the sub-daily temporal alignment of the shell element-to-calcium profiles was accomplished by linear interpolation, assigning a set number of data points to each day, as described by Yan et al. (2020, 2021) and Liu et al. (2022). Here, we applied a revised alignment technique which takes into account that the energy available for shell growth in *T. squamosa* is influenced by the photosynthetic efficiency of its zooxanthellae symbionts (Bonham, 1965; Rosewater, 1965; Griffiths and Klumpp, 1996). Thus, shell growth does not occur at a constant rate throughout the day but follows a non-linear model (Fig. 1C) which was empirically developed considering the activity patterns of photosymbiotic giant clams (Killam et al., 2023b) and the local solar cycle (average sunrise and sunset timing at the collection site). Following this model, 75 % of daily shell growth occurs between 6 am and 6 pm (daylight), with growth rate peaking at noon, while the remaining 25 % of growth occurs between 6 pm and 6 am during nighttime when the daily growth lines are formed. The highest Sr/Ca value of each day occurred in the daily growth lines and was manually assigned to midnight. The remaining data points were temporally aligned according to the non-linear growth model.

Temporal alignment of the BMU morphology data with the shell Sr/Ca profile was achieved through several steps of image processing using ImageJ. For each day, two ROIs were identified and delineated on the SEM mappings: one ROI representing the daily growth line and the other the daily growth increment (= main daily growth period), both identified by their corresponding date. An ImageJ macro (see Brosset et al., 2024) was used to save the coordinates of all pixels within each ROI, and the pixel coordinates of every BMU in the stitched SEM images were also obtained. An R script developed for this study (see Brosset et al., 2024) enabled an automatic timestamp assignment. Briefly, to integrate the non-linear growth model with the temporal alignment of BMU morphology data (Fig. 1C), the width of each ROI assigned to a daily growth increment was segmented into sub-sections. This segmentation divided the X coordinates (width) of each ROI into sub-sections corresponding to the number of Sr/Ca data points available for that increment, with widths adjusted according to the non-linear growth model (Fig. 1C). This process was repeated for each Y coordinate (height) of the SEM mapping and for each daily increment, effectively generating sub-ROIs that matched the timestamps of the Sr/Ca data. Consequently, sub-ROIs representing periods of rapid growth (e.g., 12 h) became broader than such of slower growth phases.

Subsequently, the SEM mappings were converted into matrices, with each matrix address corresponding to a pixel in the original image. In each matrix, daily sub-ROIs were indexed with unique identification numbers, and all matrix addresses for each sub-ROI were assigned to that identification number. Each pixel of a BMU was then allocated to the appropriate sub-ROI identification number based on its coordinates in the matrix. Once every pixel was assigned correctly, each BMU was assigned to the sub-ROI containing the majority of its pixels, providing a precise date and timestamp for each BMU in the SEM image. The 15 % largest BMUs within each sub-ROI were selected to facilitate further analysis, as previous studies have shown that most BMU morphological variation and its relationship with water temperature are predominantly observed in this size group (Höche et al., 2020, 2021). For each timestamp, median values of all morphometric parameters were calculated. This process yielded an Sr/Ca value and an average BMU shape (area, elongation, fractal dimension) for each timestamp, resulting in a sub-daily resolved 7-month time-series for the XB10 specimen. The number of data points collected per daily growth band (= couplet of one increment and one line) ranged from 5 to 15, leading to variability in the time represented by each data point due to the non-linear nature of shell growth. To standardize the effects of time-averaging, the dataset was resampled using linear interpolation to five data points per day at fixed timestamps (00:00, 04:48, 09:36, 14:24 and 19:02). For coherent analysis with environmental variables, SST data measured at the bivalve collection site with a 3-hour resolution (see Yan et al., 2020) was similarly resampled to match these sub-daily timestamps of the XB10 data. Alternatively, a high-pass filter was applied to the shell Sr/Ca data from the daily growth increments in order to generate a dataset (see Brosset et al., 2024) without the low-frequency component.

2.5. Statistical analysis and temperature reconstruction

Non-parametric tests were used for statistical analysis as the data from XB10 were not normally distributed (Shapiro tests, $p < 0.05$). Element chemical differences in shell properties associated with extreme events at the timescale of weather (WEEs; see Yan et al., 2020) and such unaffected by WEEs were evaluated using Mann-Whitney *U* (MWU) rank tests. MWU tests also assessed the impact of shell architecture by comparing Sr/Ca and BMU morphology data from different shell portions (daily growth lines and increments) and ultrastructure configurations (CCL-P and CCL-I; Fig. 1E), identified through SEM image visual examination. Daily variations and potential cycles of all shell properties were examined using autocorrelation analysis and MWU tests.

Linear regression was employed to explore the relationship between shell properties and SST. To compare the Sr/Ca values obtained by quantitative analyses (ICP-OES and LA-ICP-MS) and the semi-quantitative method (NanoSIMS), paired Fligner-Killeen tests were conducted to assess the equality of variances in the data. A Kruskal-Wallis test was also used to compare the results of the quantitative methods.

The NanoSIMS Sr/Ca data assigned to the daily growth increments were combined across consecutive days to match the resolutions of each quantitative method, with 4 days for LA-ICP-MS line scan, 1 week for ICP-OES and LA-ICP-MS with a 90 μm laser spot diameter, and 2 weeks for LA-ICP-MS with a 110 μm laser spot diameter. Linear regressions were then performed between the resulting Sr/Ca values and SST to compute temperature transfer functions. The precision of Sr/Ca-based temperature predictions was assessed for each sampling method and resolution, including sub-daily and daily averaged NanoSIMS Sr/Ca data, by calculating temperature prediction intervals (1σ). The accuracy of these temperature estimates was evaluated by calculating the mean absolute difference between the SST computed for each analytical method and the instrumental SST data from the XB10 collection site.

3. Results

3.1. Temporal variation of shell Sr/Ca and ultrastructure morphometry

The element chemistry and ultrastructure morphology of the studied shell varied independently over time (Fig. 2). Shell Sr/Ca ratios obtained by NanoSIMS increased by approx. 7 % during WEEs in comparison to periods of limited environmental stress (Fig. 2A). This difference in average shell Sr/Ca was statistically significant (MWU, $p < 0.001$), whereas none of the ultrastructure morphology parameters showed a significant difference between WEEs and non-WEE periods (Fig. 2C, E, G). On average, the BMUs measured 5.65 ± 0.90 μm^2 and their elongation and fractal dimension were approx. 1.83 ± 0.22 and 1.52 ± 0.02, respectively (Fig. 2C, E, G).

On a daily scale, consistent Sr/Ca cycles were observed (autocorrelation factor = 0.8, $p < 0.05$; Fig. 2B). Diurnal maxima occurred at the growth lines, with shell Sr/Ca values being approx. 54 % higher than diurnal minima (Fig. 2B). This difference was significant (MWU, $p < 0.001$) and consistent during both WEEs and more stable conditions. The ultrastructure morphology, i.e., the size, elongation and complexity of the BMUs, varied during the day (Fig. 2D, F, H). On average, BMUs observed at the daily Sr/Ca peaks were 0.59 μm^2 larger (MWU, $p < 0.001$) than those formed during the rest of the daily growth band (Fig. 2D). The corresponding difference in BMU elongation and fractal dimension was significant (MWU, $p < 0.001$) but represented less than 3 % of the variation (Fig. 2F, H). Despite these slight differences in the

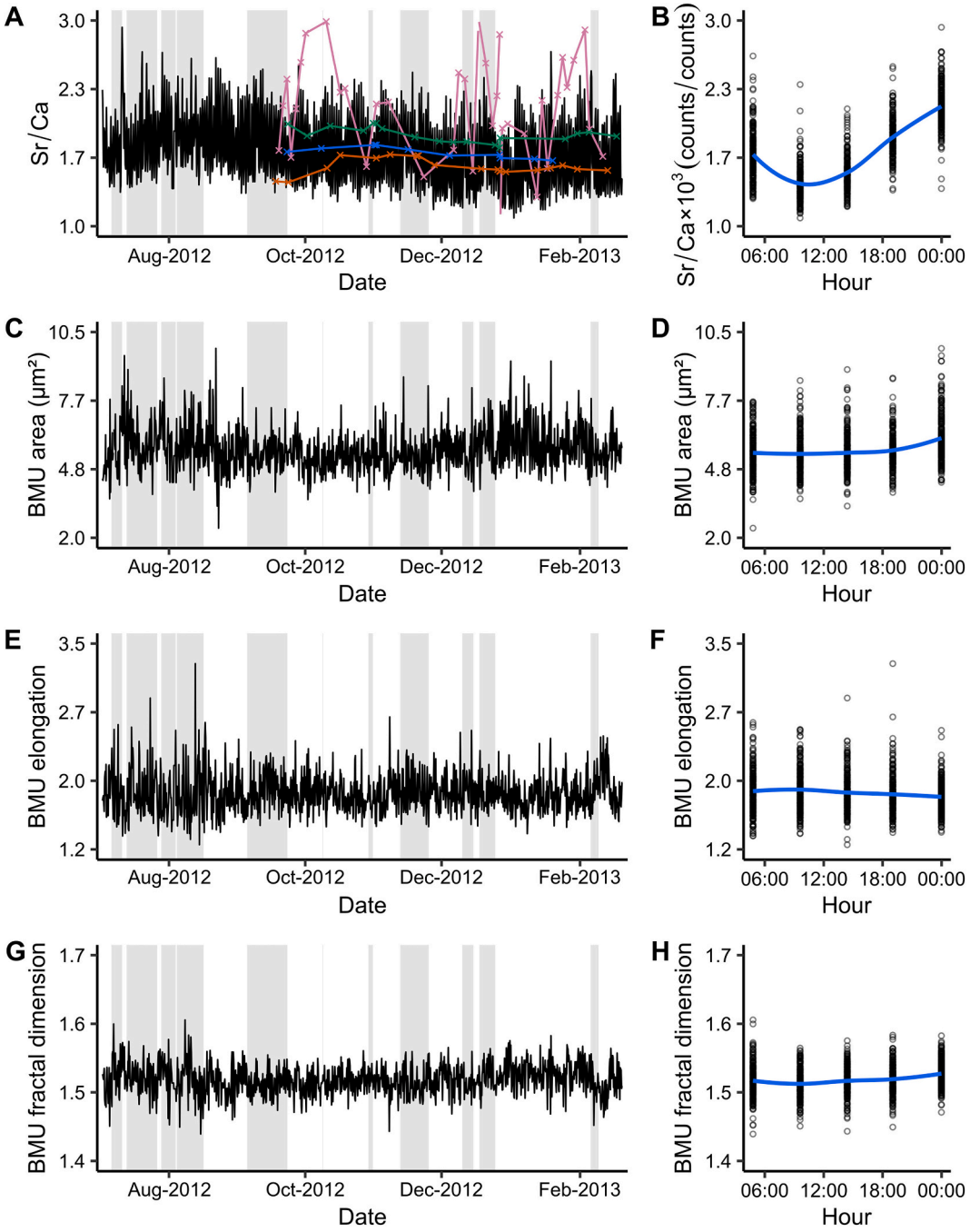

Fig. 2. Temporal variation of Sr/Ca ratios and ultrastructural properties, i.e., biomineral unit (BMU) area, elongation and fractal dimension, in the shell of the *Tridacna squamosa*. (A, C, E, G) Daily variation during a seven-month interval, with weather-scale extreme events (WEEs; details in Yan et al., 2020) indicated by grey areas. (B, D, F, H) illustrate the variation of each parameter on a sub-daily basis, with a blue line representing the average values. In (A), the black line represents Sr/Ca data measured by NanoSIMS, while the colored lines show molar Sr/Ca data based on LA-ICP-MS operated in line scan mode (pink), LA-ICP-MS operated in spot mode (90 µm spot diameter: green; 110 µm spots: blue) and ICP-OES (orange). Sr/Ca data depicted in (B) are exclusively from NanoSIMS. (For interpretation of the references to colour in this figure legend, the reader is referred to the web version of this article.)

BMU morphology of the daily growth lines and increments, none of the studied ultrastructure properties showed a clear daily cycle (autocorrelation factor < 0.2, $p < 0.05$; Fig. 2D, F, H).

In contrast to high-resolution NanoSIMS data, the sampling resolution of LA-ICP-MS and ICP-OES was too coarse to distinguish between Sr/Ca ratios in daily growth lines and increments. Data representing several days and nights of growth masked the diurnal Sr/Ca maxima. Molar Sr/Ca data varied slightly between the different quantitative methods. The highest mean and variance was obtained by LA-ICP-MS operated in line scan mode (2.17 ± 0.47 mmol/mol; Fig. 2A). Sr/Ca data measured by ICP-OES equaled 1.57 ± 0.08 mmol/mol (Fig. 2A). When measured by LA-ICP-MS in spot mode, Sr/Ca values were 1.88 ± 0.08 and 1.71 ± 0.05 mmol/mol for spot diameters of 90 and 110 µm, respectively (Fig. 2A). Furthermore, compared to the semi-quantitative shell Sr/Ca analysis (NanoSIMS), the variance of the molar Sr/Ca ratios differed significantly (Fligner-Killeen, $p < 0.001$) and also showed statistical differences between each quantitative analytical method (Kruskal-Wallis, $p < 0.001$; Fig. 2A). It should be added that the much larger variance of line scan LA-ICP-MS data compared to such obtained in spot mode results from much shorter acquisition times.

3.2. Relationship between shell properties, temperature and ultrastructure configuration

The strontium content of the *T. squamosa* shell showed a significant positive correlation with water temperature (Fig. 3A). The strongest correlation with SST was found for Sr/Ca ratios measured within the main growing portions of the shell, i.e., daily growth increments, with $R^2 = 0.36$ ($p < 0.001$; Fig. 3A). It needs to be pointed out that such correlation remained unchanged when a high-pass filter was applied to the Sr/Ca data from the daily growth increments (see also Brosset et al., 2024). Shell Sr/Ca increased by 5 % / °C during daytime (Fig. 3A). In contrast, less than 10 % of the Sr/Ca variations could be explained by temperature if only data from the growth lines were considered or when Sr/Ca ratios from the day and night (= one daily growth band) were combined ($R^2 = 0.06$ and 0.08, respectively, $p < 0.001$; Fig. 3A). Additionally, no significant relationship ($p > 0.05$) was found between SST and the morphology of the shell ultrastructure, whether the BMU area (Fig. 3B), elongation (Fig. 3C) and fractal dimension (Fig. 3D) were considered separately or combined between shell daily growth lines and increments.

Shell portions formed during WEEs showed prismatic features within the ultrastructure, i.e., CCL-P configuration (Fig. 1E), nearly 30 % more frequently than shell portions deposited during more stable growth conditions. During non-WEE periods, more than 60 % of the complex-crossed lamellar pattern of the shell was devoid of intricated prisms, i.e., the CCL-I configuration (Fig. 1E). On average, shell growth increments with a CCL-P configuration had significantly higher Sr/Ca ratios compared to those found in CCL-I increments (MWU, $p < 0.01$), although they only differed morphometrically by 2 % (Fig. 4A). The size of the BMUs was indistinguishable between CCL-I and CCL-P ultrastructural configurations ($p > 0.05$; Fig. 4B). However, BMUs from CCL-I increments were significantly (MWU, $p < 0.01$) less round (average elongation = 1.85 ± 0.22) and complex (average fractal dimension = 1.51 ± 0.02) than those found in areas with intricated prisms (average elongation = 1.80 ± 0.22 and average fractal dimension = 1.52 ± 0.02; Fig. 4C, D).

3.3. Significance of Sr/Ca-based temperature reconstructions

The correlation between shell Sr/Ca and SST was significantly stronger when NanoSIMS data were aggregated over several consecutive daily increments, compared to similar temporal resolutions obtained from LA-ICP-MS and ICP-OES analyses (Fig. 5). At a 4-day resolution, no relationship was found between molar Sr/Ca ratios and SST ($p > 0.05$; Fig. 5A), while 78 % of the Sr/Ca variance was explained by SST variation using NanoSIMS data from 4 consecutive daily increments ($p < 0.001$; Fig. 5B). Similarly, 83 % of the variance in weekly averaged increment Sr/Ca data (NanoSIMS) was explained by temperature variation ($p < 0.001$; Fig. 5D and F), with no significant relationship identified in weekly molar Sr/Ca ratios obtained via ICP-OES ($p > 0.05$; Fig. 5C). Shell Sr/Ca data from LA-ICP-MS spot analyses (90 µm and 110 µm diameters) were significantly correlated with weekly ($R^2 = 0.30$, $p < 0.02$; Fig. 5E) and bi-weekly ($R^2 = 0.50$, $p < 0.01$; Fig. 5G) SST variations, although the Sr/Ca ratios increased only by 4 and 3 % per °C, respectively. In contrast, NanoSIMS data from daily increments exhibited a temperature sensitivity of 6 % / °C across all considered temporal resolutions (Fig. 5B, D, F, H), explaining up to 86 % of the shell Sr/Ca variance by SST (Fig. 5H).

Sub-daily water temperature variation could be predicted to the nearest ± 2.8 °C using shell NanoSIMS Sr/Ca data from daily growth increments (Fig. 6A). Daily averaging narrowed the prediction interval to ± 2.2 °C (Fig. 6B). Combining data from 4, 7, and 14 consecutive daily increments further reduced the prediction intervals to ± 1.7 °C, ± 1.6 °C, and ± 1.5 °C, respectively (Fig. 6D, F, H, and J). In comparison, molar Sr/Ca ratios that included multiple daily growth bands resulted in prediction intervals of, at best, ± 2.2 °C for a weekly resolution (LA-ICP-

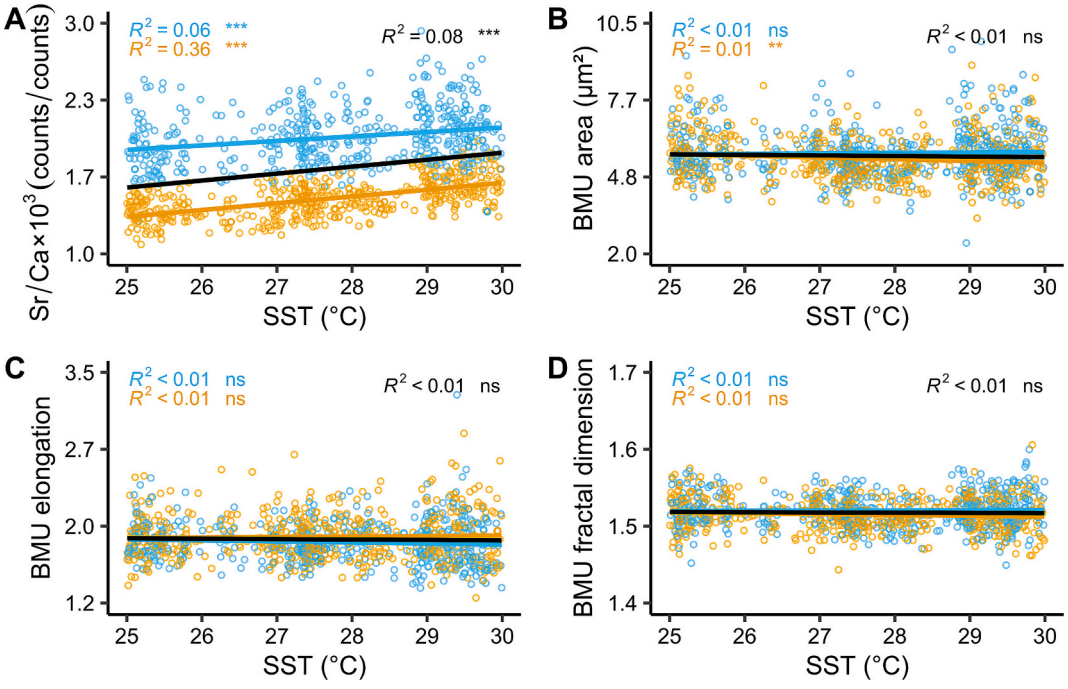

Fig. 3. Relationship between shell Sr/Ca ratios and ultrastructural properties, i.e., biomineral unit (BMU) area, elongation and fractal dimension, and sea surface temperature (SST). Blue and orange denote data from the daily growth lines and the daily increments, respectively, of studied specimen of *Tridacna squamosa*. Blue, orange and black lines stand for linear regressions computed with data from the growth lines, the increments and both growth lines and increments combined, respectively. Coefficients of determination (R^2) and significance levels are depicted for each of the linear regressions (***$p < 0.001$, **$p < 0.01$, * $p < 0.05$, and ns indicates $p > 0.05$). (A) Relationship between shell Sr/Ca and SST. (B) Relationship between BMU area and SST. (C) Relationship between BMU elongation and SST. (D) Relationship between BMU fractal dimension and SST. (For interpretation of the references to colour in this figure legend, the reader is referred to the web version of this article.)

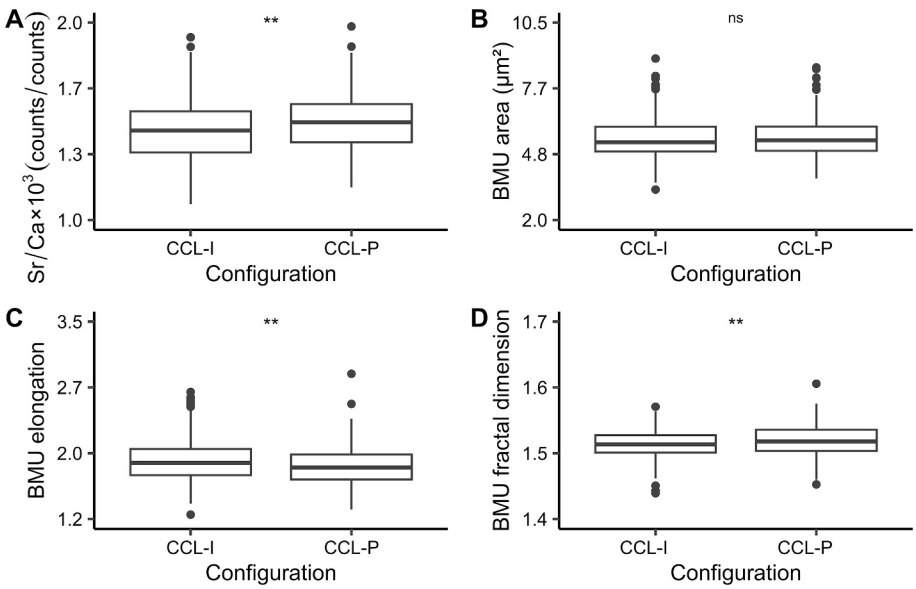

Fig. 4. Shell Sr/Ca and ultrastructural properties, i.e., biomineral unit (BMU) area, elongation and fractal dimension, from the complex crossed-lamellar (CCL) ultrastructure of the *Tridacna squamosa*. CCL-P = CCL ultrastructure with intricated prisms; CCL-I = prism-free configuration of CCL ultrastructure. (A) Shell Sr/Ca. (B) BMU area, (C) elongation and (D) fractal dimension. The bold black line represents the median, the lower and upper limits of the boxes indicate the first and third quartiles, vertical lines denote the minimum and maximum values, and black dots represent outliers. Significance of the Mann-Whitney *U* test between CCL-P and CCL-I data is depicted in each panel (***$p < 0.001$, ** $p < 0.01$, * $p < 0.05$, and ns indicates $p > 0.05$).

MS 90 µm spots; Fig. 6G) and ± 2.5 °C for a bi-weekly resolution (LA-ICP-MS 110 µm spots; Fig. 6I). The prediction models were not significant for the data obtained from a LA-ICP-MS line scan (4-day resolution; Fig. 6C) and ICP-OES (1-week resolution; Fig. 6E).

The most accurate temperature estimates from shell Sr/Ca ratios were obtained from NanoSIMS data averaged over multiple consecutive daily growth increments (Fig. 7). Bi-weekly resolved reconstructed SST differed, on average, by approx. 0.58 °C from instrumental SST, and both datasets were strongly correlated (Pearson $r = 0.93$, $p < 0.001$), showing no significant difference (MWU, $p > 0.05$). SST estimates were more accurate during WEEs or for shell portions with prismatic features (CCL-P), with an average difference of 0.48 °C and a Pearson correlation of up to 0.95 between reconstructed and instrumental SST profiles ($p < 0.001$), compared to more stable conditions or CCL-I increments, which differed by up to 0.63 °C.

4. Discussion

The meaning of Sr/Ca variations in tridacnids (and other bivalve taxa) is still a matter of debate (Yan et al., 2011; Sano et al., 2012; Warter et al., 2018; Peharda et al., 2021; DeWinter et al., 2023). Whereas on the seasonal scale, temperature seems to be negatively correlated to shell Sr/Ca of several different giant clam species (e.g., Yan et al., 2011, 2013, 2014) and positively in others including *T. squamosa* and *T. derasa* (Liu et al., 2021), such link could not be verified on shorter time-scales (e.g., in *Tridacna gigas*: Elliot et al., 2009), specifically on the diurnal time-scale (Sano et al., 2012). While Sano et al. (2012) likewise observed a negative coupling with temperature on the seasonal scale, shell Sr/Ca of *T. derasa* was also negatively correlated to seasonal changes in insolation. Furthermore, the seasonal Sr/Ca changes were as large as such between day and night despite nearly unchanged diurnal water temperature. As in the present study, Sano et al. (2012) found diurnal Sr/Ca cycles, with higher Sr/Ca values in daily growth lines (= shell portions produced during nighttime when growth rate was retarded) than in daily growth increments (= shell portions produced during the day when the photosymbionts were active and the shell was growing fast). Based on these observations, Sano et al. (2012) concluded that changes in shell Sr/Ca of giant clams are inversely correlated with light availability, both on daily and seasonal time-scales, but not temperature. However, Warter et al. (2018) found the same diurnal Sr/Ca cycles in shells of *Tridacna crocea* grown in laboratory tanks under constant illumination. These authors therefore suggested that circadian biological rhythms control the Sr incorporation into the shells rather than temperature or the light cycle. Our findings partly support this view.

4.1. Shell Sr/Ca as a temperature proxy

As indicated by the results herein, shell Sr/Ca values of *T. squamosa* are positively correlated to water temperature and can be used to reconstruct SST with an uncertainty of ± 1.5 to 2.8 °C, provided that only shell portions formed during daytime (daily growth increments) are considered (Section 3.3). This finding was possible through an ultra-high-resolution chemical analysis of the shell via NanoSIMS combined with growth pattern and ultrastructure investigations. The isolated analysis of chemical properties in daily growth lines and increments seemed advised and necessary, because in many other bivalve species, Sr levels differ markedly between ultrastructurally different shell portions: Higher Sr/Ca values were observed in growth lines, typically composed of irregular simple prisms (as in *T. squamosa*), and lower values in growth increments (made of other ultrastructures, here CCL ultrastructure). This likewise applies to daily (Füllenbach et al., 2017; Sano et al., 2012) as well as annual growth patterns (Foster et al., 2009; Schöne et al., 2011, 2013; Shirai et al., 2014).

Whereas 36 % of the Sr/Ca variation of daily growth increments could be explained by temperature, the explained variability remained below 10 % if only data from the daily growth lines were considered or data from both daily increments and lines were combined (Section 3.2). Noteworthy, all correlations were statistically highly significant ($p < 0.001$), despite a large proportion of the variance being unrelated to SST fluctuations but rather linked to the bivalve physiology and/or variations in its ecosystem. Therefore, the transfer functions for Sr/Ca data on the sub-daily time-scale come with a relatively large uncertainty of ± 2.8 °C (Section 3.3) that may limit applications in tropical regions where the seasonal temperature amplitude is barely larger than that. This uncertainty can be cut in half (± 1.5 °C) if biweekly SST averages are

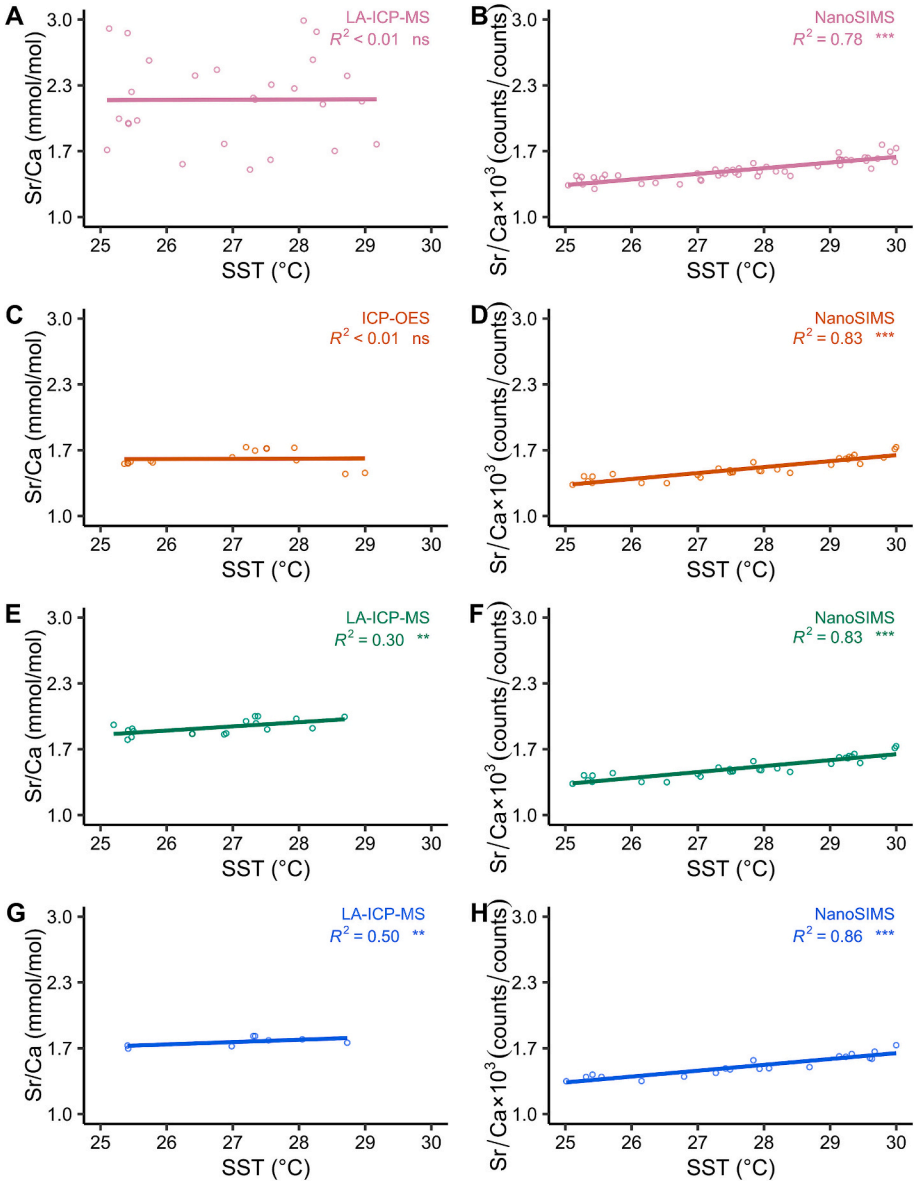

Fig. 5. Relationship between shell Sr/Ca (*Tridacna squamosa*) and sea surface temperature (SST). (A) Molar Sr/Ca data obtained by LA-ICP-MS operated in line scan mode (4-day resolution) and (B) corresponding (down-sampled) NanoSIMS data from the daily growth increments. (C) Weekly resolved molar Sr/Ca data obtained by ICP-OES and (D) corresponding (down-sampled) NanoSIMS data from the daily growth increments. (E) Weekly resolved molar Sr/Ca data obtained by LA-ICP-MS operated in spot mode (spot diameter: 90 μm) and (F) corresponding (down-sampled) NanoSIMS data from the daily growth increments. (G) Bi-weekly resolved molar Sr/Ca data obtained by LA-ICP-MS operated in spot mode (spot diameter: 110 μm) and (H) corresponding (down-sampled) NanoSIMS data from the daily growth increments. Coefficients of determination (R^2) and significance levels are depicted for each of the linear regressions (*** $p < 0.001$, ** $p < 0.01$, * $p < 0.05$, and ns indicating $p > 0.05$).

computed from Sr/Ca data of daily increments (Section 3.3). Through this averaging, Sr/Ca variations between days were smoothed and short-term environmental fluctuations eliminated. Consequently, the range of Sr/Ca data was smaller, leading to a stronger correlation of shell Sr/Ca with SST (Fig. 5B, D, F, H) and narrower prediction intervals of the water temperature (Fig. 6D, F, H, J). The broader prediction intervals and weaker correlation obtained at higher resolution, i.e., on sub-daily and daily time-scales (Fig. 6A, B), were likely caused by short-term environmental and/or physiological fluctuations affecting shell Sr/Ca ratios.

In *Arctica islandica* and *Mytilus edulis*, shell Sr/Ca and temperature were likewise weakly correlated, but the sign, slope and intercept varied significantly between localities (and environmental conditions) and ultrastructurally different shell portions (Wanamaker et al., 2008; Schöne et al., 2013; Brosset et al., 2023). This variability was associated with strong biological control over the biomineralization process and trace element incorporation as well as other factors such as salinity (Dodd and Crisp, 1982; Yan et al., 2013), growth rate (Carré et al., 2006) and food intake (Goodwin et al., 2013; Piwoni-Piórewicz et al., 2021). All such influences can result in a lower correlation between Sr/Ca and water temperature regardless of the sampling resolution. The differences observed across the range of resolutions (Section 3.3) suggest that while shell Sr/Ca of *Tridacna* spp. captures temperature trends, especially when accounting for shell architectural heterogeneity, they are also influenced by other environmental factors operating on the sub-daily scale (Sano et al., 2012; Warter et al., 2018; Yan et al., 2020; Liu et al., 2021).

Sr/Ca increased by ca. 5 % per °C (Fig. 2A). The rate of change is similar to that reported from other tridacnids (Yan et al., 2014, 2015) as well as other biogenic archives (Beck et al., 1992; Sun et al., 2004; Corrège, 2006; Schöne et al., 2013), but comes with the opposite sign.

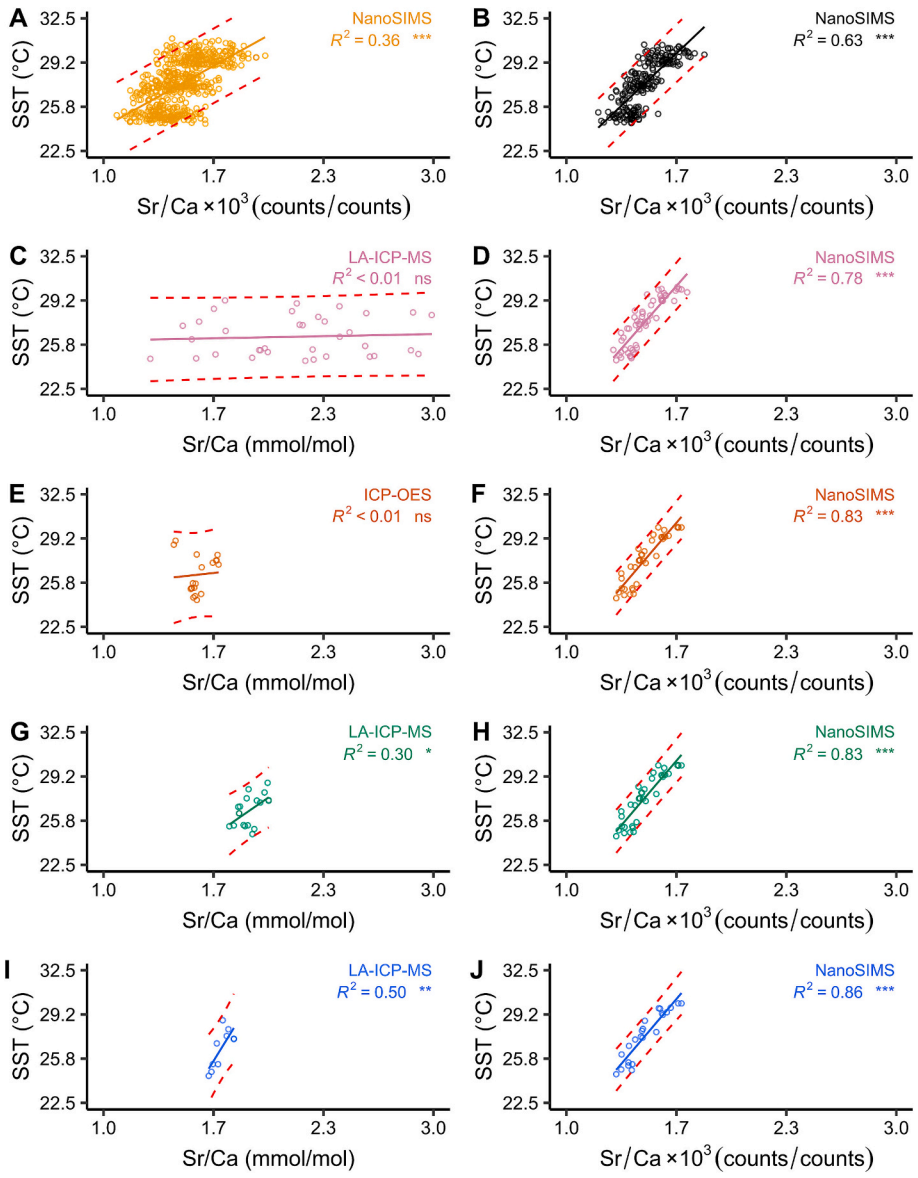

Fig. 6. Sea surface temperature (SST) reconstructed from shell Sr/Ca ratios of studied *Tridacna squamosa* specimen. Linear regression (solid lines) with 95 % prediction intervals (dashed red lines). (A + B) SST computed from NanoSIMS Sr/Ca data determined in daily growth increments (A = raw, B = daily averages). (C) SST predicted from Sr/Ca data (mmol/mol) measured by LA-ICP-MS in line scan mode (4-day resolution) and (D) corresponding SST computed from down-sampled NanoSIMS data of the daily growth increments. (E) Weekly SST predicted from ICP-OES Sr/Ca data and (F) corresponding SST computed from down-sampled NanoSIMS data of the daily growth increments. (G) Weekly SST calculated from Sr/Ca measured by LA-ICP-MS in spot mode (90 μm laser spots) and (H) corresponding SST derived from down-sampled NanoSIMS data of the daily growth increments. (I) Biweekly SST predicted from Sr/Ca data measured by LA-ICP-MS in spot mode (110 μm laser spots) and (J) corresponding SST inferred from down-sampled NanoSIMS of the daily growth increments. (For interpretation of the references to colour in this figure legend, the reader is referred to the web version of this article.)

The positive correlation between temperature and shell Sr/Ca ratios as well as the temperature sensitivity of shell Sr/Ca of *T. squamosa* reported herein is consistent with thermodynamic principles (temperature sensitivity: 4 % / °C; Gaetani and Cohen, 2006). Strontium ions (Sr^{2+}) can substitute for calcium ions (Ca^{2+}) with minimal distortions in the crystal lattice of aragonite (Gaetani and Cohen, 2006) because their ionic radii are similar (Ca^{2+} = 1.18 Å, Sr^{2+} = 1.31 Å in a 9-fold coordination, Shannon, 1976). Higher temperatures not only favor larger distortions of the crystal lattice but also increase the kinetic energy of ions in the biomineralizing environment and thus facilitate the diffusion of Sr^{2+} into the aragonite at the calcifying front (Gaetani and Cohen, 2006; Menadakis et al., 2008).

However, the absolute Sr/Ca values of *T. squamosa* are higher (between approx. 1.57 and 2.17 mmol/mol; Fig. 2A) than thermodynamically expected (approx. 1.3 mmol/mol at 25 °C; Gaetani and Cohen, 2006). Possibly, this difference can be explained with the surface entrapment model discussed by Gaetani and Cohen (2006). Following this model, aragonite crystal growth can outpace the ion diffusion rate required for equilibrium partitioning with the calcifying fluid (Watson, 1996, 2004). This mechanism leads to the entrapment of additional Sr^{2+} at the near-surface of the aragonite crystals (Watson, 1996, 2004; Gaetani and Cohen, 2006).

4.2. Shell element chemistry and ultrastructural dynamics

In *T. squamosa*, the shell element chemistry and ultrastructure morphology varied independently over time (Section 3.1). For instance, shell Sr/Ca increased significantly when the complex crossed-lamellar

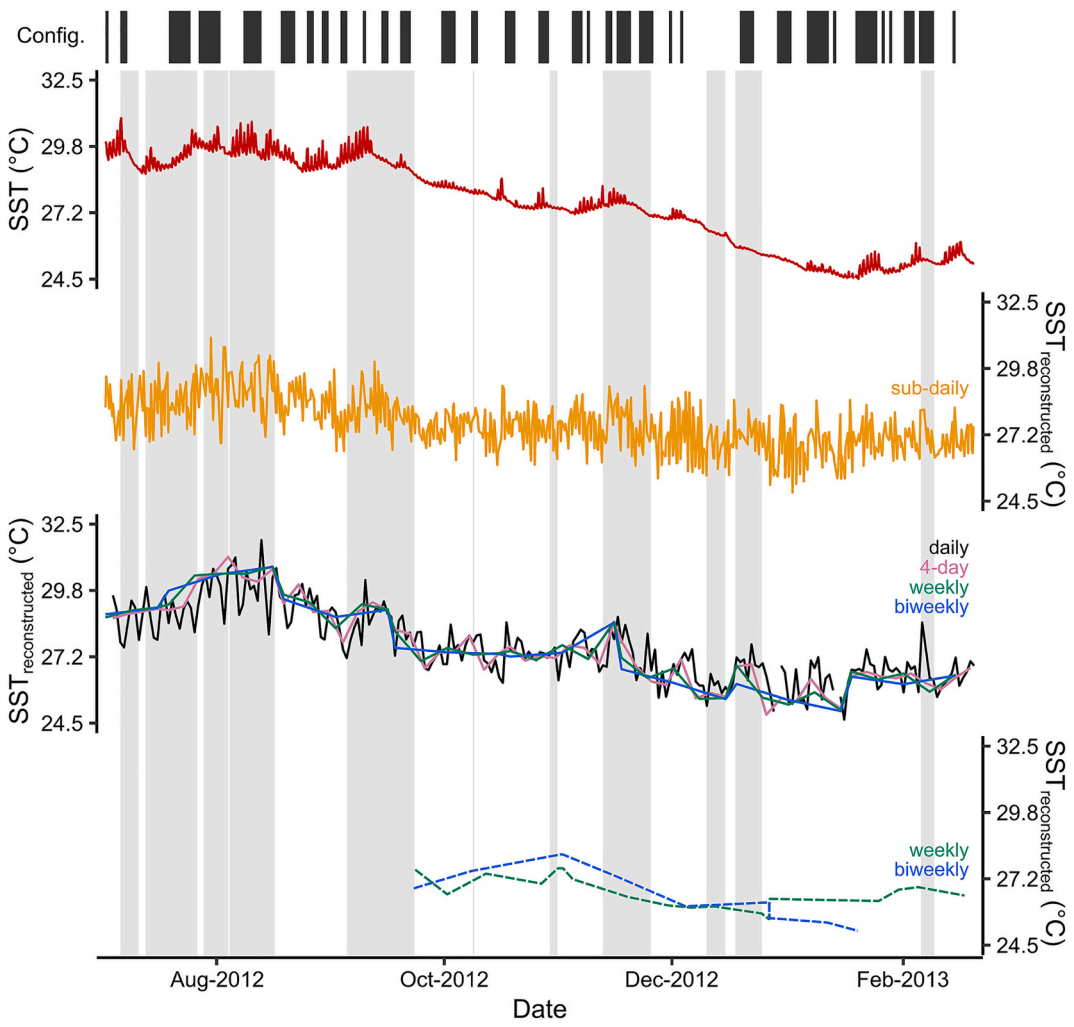

Fig. 7. Temporal variation of sea surface temperature (SST) measured at the site where the studied *Tridacna squamosa* specimen lived in comparison to average SST reconstructed from shell Sr/Ca ratios. Weather-scale extreme events (WEEs; for details see Yan et al., 2020) are indicated by grey areas. The solid red line represents instrumental SST data, while the other solid lines show SST reconstructed from NanoSIMS Sr/Ca data of the daily growth increments. SST reconstructions based on LA-ICP-MS Sr/Ca data are depicted as dashed lines. Sub-daily SST estimates are shown in orange, daily in black, 4-day resolution in pink, weekly resolved data in green and biweekly data in blue. The top portion illustrates the configuration (Config.) of the complex crossed-lamellar (CCL) ultrastructure (CCL-P = CCL with intricated prisms = black, CCL without prisms = white). (For interpretation of the references to colour in this figure legend, the reader is referred to the web version of this article.)

ultrastructure contained prisms (CCL-P; Fig. 4A). Notably, this ultrastructural modification only resulted in a 2 % change of the BMU shape and complexity (Fig. 4C, D) and no change in BMU size (Fig. 4B). Similarly, the consistent diurnal cycles of shell Sr/Ca (Fig. 2B) contrasted with the lack of corresponding fluctuations in BMU morphology (Fig. 2D, F, H). Instead, the shape of BMUs differed significantly between portions grown during daytime and nighttime ($p < 0.001$; Fig. 2D, F, H). The asynchrony between element chemical and ultrastructural dynamics suggests that both shell Sr/Ca ratios and BMU morphology are influenced by common physiological factors rather than being directly linked. While the Sr/Ca variability was partly attributable to temperature fluctuations (Sections 3.2, 3.3, and 4.1), none of the BMU morphology parameters correlated with SST (Fig. 2B, C, D), contrary to the results of ultrastructural analyses performed in some other bivalve species (*A. islandica* and *Glycymeris bimaculata*; Höche et al., 2020, 2021). This suggests that these shell properties are driven by different factors in *T. squamosa*, and while SST is a key determinant of the shell ultrastructure in non-photosymbiotic bivalves (Höche et al., 2020, 2021, 2022), light conditions likely prevail over water temperature as the primary control in photosymbiotic species like tridacnids.

In adult tridacnid specimens, most of the energy used to regulate physiological processes derives from their symbiotic relationship with photosynthetic organisms (Bonham, 1965; Rosewater, 1965; Klumpp and Lucas, 1994; Griffiths and Klumpp, 1996), i.e., zooxanthellae symbionts hosted in the mantle of the bivalve (Ip et al., 2017). During daytime, when light is available, the bivalve is active and valves are gaping (Killam et al., 2023b), maximizing symbiont exposure to sunlight and enhancing photosynthetic efficiency (Ip and Chew, 2021). As a consequence, more nutrients are available for the animal (Killam et al., 2023a) which propel its metabolic rates (Ip and Chew, 2021). Under such favorable growth conditions, the shell grows fast in association to the formation of small and elongated BMUs (Fig. 2D, F), typically found in the CCL ultrastructure of *Tridacna* spp. (Agbaje et al., 2017; Mills et al., 2024a). During daytime, the bivalve also has more energy available to actively preclude trace impurities from ending up in the shell, such as unwanted Sr^{2+} ions. Since protein and gene expression levels related to calcification processes in *Tridacna* spp. are enhanced by insolation (Ip et al., 2015, 2017), light exposure likely facilitates biomineralization through increased activity of the Ca^{2+}-ATPase transport. These processes result in lower shell Sr/Ca ratios during daytime than during night (Fig. 2B). At night, the cessation of photosynthesis leads to decreased metabolic rates and energy levels (Klumpp and Lucas, 1994),

also favored by the predator avoidance strategy of the bivalve (partial mantle retraction; Johnson et al., 2017) and manifested by a reduced nocturnal activity (Killam et al., 2023b). Slower shell growth occurring during nighttime resulted in larger BMUs (Fig. 2D). The combination of slow growth and low energy availability resulted in diurnal Sr/Ca maxima at the daily growth lines (Fig. 2B). On the daily time-scale, the offset between chemical and ultrastructural dynamics – with Sr/Ca showing a clear cyclic pattern and BMU morphology simply varying with the prevailing shell architecture – suggests that while Sr/Ca is influenced to some degree by SST and insolation, BMU morphology seems to be ultimately (and primarily) driven by the availability of light (Gannon et al., 2017) and the energy provided by the photosymbionts.

Temperature and solar irradiance are coupled variables, and while they seem to independently affect the shell properties of *T. squamosa*, changes in insolation lead to fluctuations of the water temperature. During daytime, favorable weather causes a gradual increase in SST, but due to the thermal inertia of water, SST decreases more slowly than insolation at the end of the day (Gentemann et al., 2003; Sano et al., 2012). The gradual temperature decline likely explains the continuous variation of shell Sr/Ca during the day, while the more abrupt ultrastructural difference between daytime and nighttime would primarily reflect distinct differences of light availability.

Diurnal Sr/Ca cycles were also observed in shells of tridacnids cultured under constant illumination (Warter et al., 2018) and constant water temperature (Sano et al., 2012). Although these studies did not explicitly consider changes of the shell architecture, they confirm that variations in SST and light availability do not fully explain the Sr/Ca variability in giant clam shells. In the specimen investigated here, for which the potential impact of shell ultrastructure was considered, diurnal Sr/Ca cycles persisted during WEEs and at times during which the typical ultrastructural pattern (prisms at the daily growth lines and CCL-I in daily growth increments) was replaced by CCL-P. Thus, diurnal shell Sr/Ca cycles are not only influenced by SST and insolation but most likely also by a biological clock, as suggested by Warter et al. (2018) and DeWinter et al. (2023), and other physiological changes. For instance, when illuminated, the photosymbionts of *T. squamosa* regulate and absorb the host metabolic waste, as indicated by higher levels of proteins involved in ammonia transport (Pang et al., 2022). This process may signal favorable growth conditions to the host and likely promotes the formation of daily increments during daytime through the conversion of ammonia into amino acids, ultimately providing organic components essential for $CaCO_3$ deposition (Teh et al., 2021).

4.3. Implications of shell element chemical and ultrastructural dynamics for proxy studies

As demonstrated here, to properly interpret the meaning of shell Sr/Ca variations, it is crucial to consider the shell architecture of *Tridacna* spp., or more specifically, the time during which they grow, day or night. Sr is heterogeneously distributed across the daily growth bands of the fluted giant clam, i.e., enriched in the daily growth lines and depleted in the increments (Fig. 2B). NanoSIMS analysis (spot size = 2 μm^2) was essential to isolate data from shell portions grown during daytime. In the studied specimen, the average daily growth band measured 18.5 μm in width (Yan et al., 2020), with most shell material deposited during daytime (= daily growth increment) and only a small fraction at night (= daily growth line). The automated temporal alignment method developed in this study, enabled by high-resolution chemical and ultrastructural analyses (Sections 2.2, 2.3, 2.4 and 2.5), addressed the limitations of coarser-resolution sampling methods such as LA-ICP-MS and ICP-OES. These methods provided a time-averaging of 4 to 14 days per data point (45 to 150 μm), which is much broader than the daily growth band width of the studied species (approx. 18.5 μm). This sampling resolution is evidently too coarse to isolate data from daily growth increments. It should be noted that coarser-resolution sampling methods may bias quantitative Sr/Ca data towards lower molar ratios, because shell portions formed during daytime are over-represented in each data point in comparison to shell material deposited at night due to the architectural heterogeneity of the shell daily growth bands. Therefore, the ultra-high-resolution approach used in this study can refine the interpretation of shell Sr/Ca profiles in *T. squamosa* and would be applicable to other bivalve species that grow sufficiently fast.

A detailed analysis of the studied specimen revealed distinct ultrastructural configurations, likely resulting from environmental stress. Specifically, prismatic features within the CCL ultrastructure (CCL-P) were more frequent during weather extremes and had significantly higher Sr/Ca values (Fig. 4A). Complex ultrastructural patterns in *Tridacna* spp. shells are known to enhance the mechanical resistance of the shell material (Agbaje et al., 2017), suggesting that the formation of the complex BMUs found in CCL-P (Fig. 4D) was triggered by unfavorable growth conditions. This could indicate a biologically mediated adaptation of the bivalve to withstand variable environmental conditions (Agbaje et al., 2017; Gannon et al., 2017; Mills et al., 2024b). Furthermore, temperature reconstructions using Sr/Ca data from CCL-P shell portions or those grown during WEEs were in better agreement with instrumental SST than those of CCL-I shell portions and times without extreme weather events (Fig. 7). This suggests that the biological control over strontium incorporation into the shell decreases under less favorable growth conditions, leading to more accurate SST reconstructions. In tropical environments, such as reefs where *T. squamosa* lives, temperature variations seem to lack sufficient magnitude to cause significant changes in shell Sr/Ca compared to times of increased physiological stress. Furthermore, since CCL-P appears to be associated with WEEs, the occurrence of such ultrastructure could serve as a useful tool in paleoweather research to identify episodes of environmental stress.

While the methods developed in this study offer potential for future research, it is important to note that the observed variations in element chemistry and ultrastructural configurations may be species-specific responses to environmental stress. *T. squamosa* is one of the most widely distributed giant clam species (bin Othman et al., 2010). It can inhabit a range of water depths (Jantzen et al., 2008) and rely on various levels of autotrophic and heterotrophic energy sources (Klumpp and Griffiths, 1994; Jantzen et al., 2008), displaying great flexibility to fluctuations in its environment. For example, the presence of CCL-P in the shell of *T. squamosa* is correlated to increased water turbidity and results in lower Sr/Ca levels compared to CCL-I (Mills et al., 2024b), contrasting with our findings and likely reflecting the remarkable plasticity of this species. Future research aimed at reconstructing seawater temperature using Sr/Ca ratios from tridacnid shells should prioritize species-specific studies of shell properties (element chemistry and ultrastructure) using ultra-high-resolution methods. Culture experiments would also allow to generate precise sub-daily species-specific shell growth models, which could be used to refine the Sr/Ca thermometer. Furthermore, such experiments could shed light on the actual influence of environmental variables such as water temperature, turbidity and insolation on the element chemical and ultrastructural properties of the shells. All this could improve the understanding of the adaptive responses of tridacnids to changing environments and open new perspectives for paleoclimate research.

5. Summary and conclusions

This study explored the complex relationships between environmental conditions and both shell Sr/Ca and ultrastructure properties of *Tridacna squamosa*. The results highlighted the potential of shell Sr/Ca as a proxy for sea surface temperature. Significant correlations were only observed between water temperature and Sr/Ca ratios of the daily growth increments. Ultra-high-resolution analytical techniques (NanoSIMS and SEM) were essential to isolate such data, thereby improving temperature reconstructions. The observed positive relationship between shell Sr/Ca and SST aligns with thermodynamic predictions and

confirms the potential of the Sr/Ca thermometer in shells of *T. squamosa*. Upcoming studies should check if the same applies to other tridacnid species. The results of this study also suggest that shell Sr/Ca and ultrastructural properties are not directly linked but are instead both driven by underlying physiological processes. While Sr/Ca values were influenced by both light availability and SST, BMU morphology seemed to be primarily driven by insolation due to the photosynthetic activity of the symbionts. Ultrastructural changes probably reflect diurnal variations in metabolic rate. Furthermore, distinct ultrastructural patterns, namely the CCL ultrastructure with intricated prisms (CCL-P) were formed during massive environmental stress and may provide valuable insights into the frequency of paleo-weather extremes.

CRediT authorship contribution statement

Cornélia Brosset: Writing – review & editing, Writing – original draft, Visualization, Validation, Methodology, Investigation, Formal analysis, Data curation, Conceptualization. **Chengcheng Liu:** Writing – review & editing, Resources, Funding acquisition. **Haotian Yang:** Writing – review & editing, Resources. **Hong Yan:** Writing – review & editing, Resources, Project administration, Funding acquisition. **Bernd R. Schöne:** Writing – review & editing, Writing – original draft, Validation, Supervision, Resources, Project administration, Investigation, Funding acquisition, Conceptualization.

Declaration of competing interest

The authors declare that they have no known competing financial interests or personal relationships that could have appeared to influence the work reported in this paper.

Data availability

The datasets presented in this study can be found in online repositories. The names of the repository/repositories and accession number(s) can be found below: Brosset et al., 2024 (https://zenodo.org/records/12206690).

Acknowledgements

This work was supported by a grant to BRS and HY by the Sino-German Center for Research Promotion [M-0163] and to CL and HY by the National Natural Science Foundation of China (NSFC) [42103084]. We thank the editor and two anonymous reviewers for their time and valuable feedback.

References

Agbaje, O.B.A., Wirth, R., Morales, L.F.G., Shirai, K., Kosnik, M., Watanabe, T., Jacob, D. E., 2017. Architecture of crossed-lamellar bivalve shells: the southern giant clam (*Tridacna derasa*, Röding, 1798). R. Soc. Open Sci. 4, 170622. https://doi.org/10.1098/rsos.170622.

Aharon, P., 1983. 140,000-yr isotope climatic record from raised coral reefs in New Guinea. Nature 304, 720–723. https://doi.org/10.1038/304720a0.

Aharon, P., Chappell, J., 1986. Oxygen isotopes, sea level changes and the temperature history of a coral reef environment in New Guinea over the last 105 years. Palaeogeogr. Palaeoclimatol. Palaeoecol. 56, 337–379. https://doi.org/10.1016/0031-0182(86)90101-X.

Arias-Ruiz, C., Elliot, M., Bézos, A., Pedoja, K., Husson, L., Cahyarini, S.Y., Cariou, E., Michel, E., La, C., Manssouri, F., 2017. Geochemical fingerprints of climate variation and the extreme La Niña 2010–11 as recorded in a *Tridacna squamosa* shell from Sulawesi, Indonesia. Palaeogeogr. Palaeoclimatol. Palaeoecol. 487, 216–228. https://doi.org/10.1016/j.palaeo.2017.08.037.

Arndt, I., Coenen, D., Evans, D., Renema, W., Müller, W., 2023. Quantifying sub-seasonal growth rate changes in fossil giant clams using wavelet transformation of daily Mg/Ca cycles. Geochem. Geophys. Geosyst. 24. https://doi.org/10.1029/2023GC010992 e2023GC010992.

Ballesta-Artero, I., Witbaard, R., Carroll, M.L., Van Der Meer, J., 2017. Environmental factors regulating gaping activity of the bivalve *Arctica islandica* in Northern Norway. Mar. Biol. 164, 116. https://doi.org/10.1007/s00227-017-3144-7.

Barrat, J.-A., Chauvaud, L., Olivier, F., Poitevin, P., Rouget, M.-L., 2023. Trace elements in bivalve shells: how "vital effects" can bias environmental studies. Chem. Geol. 121695. https://doi.org/10.1016/j.chemgeo.2023.121695.

Beck, J.W., Edwards, R.L., Ito, E., Taylor, F.W., Recy, J., Rougerie, F., Joannot, P., Henin, C., 1992. Sea-Surface Temperature from coral skeletal Strontium/Calcium ratios. Science 257, 644–647. https://doi.org/10.1126/science.257.5070.644.

Bin Othman, A.S., Goh, G.H., Todd, P.A., 2010. The distribution and status of giant clams (family Tridacnidae) – a short review. Raffles Bull. Zool. 58, 103–111. https://doi.org/10.5281/zenodo.5342460.

Bogovic, J.A., Hanslovsky, P., Wong, A., Saalfeld, S., 2016. Robust registration of calcium images by learned contrast synthesis. In: 2016 IEEE 13th International Symposium on Biomedical Imaging (ISBI). Presented at the 2016 IEEE 13th International Symposium on Biomedical Imaging (ISBI 2016). IEEE, Prague, Czech Republic, pp. 1123–1126. https://doi.org/10.1109/ISBI.2016.7493463.

Bonham, K., 1965. Growth rate of giant clam *Tridacna gigas* at Bikini Atoll as revealed by radioautography. Science 149, 300–302. https://doi.org/10.1126/science.149.3681.300.

Brosset, C., Höche, N., Shirai, K., Nishida, K., Mertz-Kraus, R., Schöne, B.R., 2022. Strong coupling between biomineral morphology and Sr/Ca of *Arctica islandica* (Bivalvia) – implications for shell Sr/Ca-based temperature estimates. Minerals 12, 500. https://doi.org/10.3390/min12050500.

Brosset, C., Höche, N., Witbaard, R., Nishida, K., Shirai, K., Mertz-Kraus, R., Schöne, B.R., 2023. Sr/Ca in shells of laboratory-grown bivalves (*Arctica islandica*) serves as a proxy for water temperature – Implications for (paleo)environmental research? Front. Mar. Sci. 10, 1279164. https://doi.org/10.3389/fmars.2023.1279164.

Brosset, C., Liu, C., Yang, H., Yan, H., Schöne, B.R., 2024. Data for "Integrating high-resolution Sr/Ca and ultrastructural analyses of the *Tridacna squamosa* shell to reconstruct sub-daily seawater temperature variation" https://doi.org/10.5281/zenodo.12206690.

Butler, P.G., Wanamaker, A.D., Scourse, J.D., Richardson, C.A., Reynolds, D.J., 2013. Variability of marine climate on the North Icelandic Shelf in a 1357-year proxy archive based on growth increments in the bivalve *Arctica islandica*. Palaeogeogr. Palaeoclimatol. Palaeoecol. 373, 141–151. https://doi.org/10.1016/j.palaeo.2012.01.016.

Carré, M., Bentaleb, I., Bruguier, O., Ordinola, E., Barrett, N.T., Fontugne, M., 2006. Calcification rate influence on trace element concentrations in aragonitic bivalve shells: evidences and mechanisms. Geochim. Cosmochim. Acta 70, 4906–4920. https://doi.org/10.1016/j.gca.2006.07.019.

Carré, M., Sachs, J.P., Schauer, A.J., Rodrguez, W.E., Ramos, F.C., 2013. Reconstructing El Niño-Southern Oscillation activity and ocean temperature seasonality from short-lived marine mollusk shells from Peru. Palaeogeogr. Palaeoclimatol. Palaeoecol. 371, 45–53. https://doi.org/10.1016/j.palaeo.2012.12.014.

Chauvaud, L., Thouzeau, G., Paulet, Y.-M., 1998. Effects of environmental factors on the daily growth rate of *Pecten maximus* juveniles in the Bay of Brest (France). J. Exp. Mar. Biol. Ecol. 227, 83–111. https://doi.org/10.1016/S0022-0981(97)00263-3.

Clark, G.R., 2005. Daily growth lines in some living Pectens (Mollusca: Bivalvia), and some applications in a fossil relative: time and tide will tell. Palaeogeogr. Palaeoclimatol. Palaeoecol. 228, 26–42. https://doi.org/10.1016/j.palaeo.2005.03.044.

Corrège, T., 2006. Sea surface temperature and salinity reconstruction from coral geochemical tracers. Palaeogeogr. Palaeoclimatol. Palaeoecol. 232, 408–428. https://doi.org/10.1016/j.palaeo.2005.10.014.

DeWinter, N.J., Dämmer, L.K., Falkenroth, M., Reichart, G.-J., Moretti, S., Martínez-García, A., Höche, N., Schöne, B.R., Rodiouchkina, K., Goderis, S., Vanhaecke, F., Van Leeuwen, S.M., Ziegler, M., 2021. Multi-isotopic and trace element evidence against different formation pathways for oyster microstructures. Geochim. Cosmochim. Acta 308, 326–352. https://doi.org/10.1016/j.gca.2021.06.012.

DeWinter, N.J., Killam, D., Fröhlich, L., De Nooijer, L., Boer, W., Schöne, B.R., Thébault, J., Reichart, G.-J., 2023. Ultradian rhythms in shell composition of photosymbiotic and non-photosymbiotic mollusks. Biogeosciences 20, 3027–3052. https://doi.org/10.5194/bg-20-3027-2023.

Dodd, J.R., Crisp, E.L., 1982. Non-linear variation with salinity of Sr/Ca and Mg/Ca ratios in water and aragonitic bivalve shells and implications for paleosalinity studies. Palaeogeogr. Palaeoclimatol. Palaeoecol. 38, 45–56. https://doi.org/10.1016/0031-0182(82)90063-3.

Elliot, M., Welsh, K., Chilcott, C., McCulloch, M., Chappell, J., Ayling, B., 2009. Profiles of trace elements and stable isotopes derived from giant long-lived *Tridacna gigas* bivalves: potential applications in paleoclimate studies. Palaeogeogr. Palaeoclimatol. Palaeoecol. 280, 132–142. https://doi.org/10.1016/j.palaeo.2009.06.007.

Epstein, S., Buchsbaum, R., Lowenstam, H.A., Urey, H.C., 1953. Revised carbonate-water isotopic temperature scale. Geol. Soc. Am. Bull. 64, 1315. https://doi.org/10.1130/0016-7606(1953)64[1315:RCITS]2.0.CO;2.

Foster, L.C., Allison, N., Finch, A.A., Andersson, C., 2009. Strontium distribution in the shell of the aragonite bivalve *Arctica islandica*. Geochem. Geophys. Geosyst. 10, 1–14. https://doi.org/10.1029/2007GC001915.

Fritz, L.W., Haven, D.S., 1983. Hard clam, *Mercenaria mercenaria*: shell growth patterns in Chesapeake Bay. Fish. Bull. 81, 697–708.

Füllenbach, C.S., Schöne, B.R., Mertz-Kraus, R., 2015. Strontium/lithium ratio in aragonitic shells of *Cerastoderma edule* (Bivalvia) – a new potential temperature proxy for brackish environments. Chem. Geol. 417, 341–355. https://doi.org/10.1016/j.chemgeo.2015.10.030.

Füllenbach, C.S., Schöne, B.R., Shirai, K., Takahata, N., Ishida, A., Sano, Y., 2017. Minute co-variations of Sr/Ca ratios and microstructures in the aragonitic shell of *Cerastoderma edule* (Bivalvia) – are geochemical variations at the ultra-scale masking potential environmental signals? Geochim. Cosmochim. Acta 205, 256–271. https://doi.org/10.1016/j.gca.2017.02.019.

Gaetani, G.A., Cohen, A.L., 2006. Element partitioning during precipitation of aragonite from seawater: a framework for understanding paleoproxies. Geochim. Cosmochim. Acta 70, 4617–4634. https://doi.org/10.1016/j.gca.2006.07.008.

Gannon, M.E., Pérez-Huerta, A., Aharon, P., Street, S.C., 2017. A biomineralization study of the Indo-Pacific giant clam *Tridacna gigas*. Coral Reefs 36, 503–517. https://doi.org/10.1007/s00338-016-1538-5.

Gentemann, C.L., Donlon, C.J., Stuart-Menteth, A., Wentz, F.J., 2003. Diurnal signals in satellite sea surface temperature measurements. Geophys. Res. Lett. 30. https://doi.org/10.1029/2002GL016291, 2002GL016291.

Goodwin, D.H., Gillikin, D.P., Roopnarine, P.D., 2013. Preliminary evaluation of potential stable isotope and trace element productivity proxies in the oyster *Crassostrea gigas*. Palaeogeogr. Palaeoclimatol. Palaeoecol. 373, 88–97. https://doi.org/10.1016/j.palaeo.2012.03.034.

Griffiths, C., Klumpp, D., 1996. Relationships between size, mantle area and zooxanthellae numbers in five species of giant clam (Tridacnidae). Mar. Ecol. Prog. Ser. 137, 139–147. https://doi.org/10.3354/meps137139.

Höche, N., Peharda, M., Walliser, E.O., Schöne, B.R., 2020. Morphological variations of crossed-lamellar ultrastructures of *Glycymeris bimaculata* (Bivalvia) serve as a marine temperature proxy. Estuar. Coast. Shelf Sci. 237, 106658. https://doi.org/10.1016/j.ecss.2020.106658.

Höche, N., Walliser, E.O., de Winter, N.J., Witbaard, R., Schöne, B.R., 2021. Temperature-induced microstructural changes in shells of laboratory-grown *Arctica islandica* (Bivalvia). PLoS One 16, e0247968. https://doi.org/10.1371/journal.pone.0247968.

Höche, N., Walliser, E.O., Schöne, B.R., 2022. Microstructural mapping of *Arctica islandica* shells reveals environmental and physiological controls on biomineral size. Front. Earth Sci. 9, 781305. https://doi.org/10.3389/feart.2021.781305.

Hori, M., Sano, Y., Ishida, A., Takahata, N., Shirai, K., Watanabe, T., 2015. Middle Holocene daily light cycle reconstructed from the strontium/calcium ratios of a fossil giant clam shell. Sci. Rep. 5, 8734. https://doi.org/10.1038/srep08734.

Ip, Y.K., Chew, S.F., 2021. Light-dependent phenomena and related molecular mechanisms in giant clam-dinoflagellate associations: a review. Front. Mar. Sci. 8, 627722. https://doi.org/10.3389/fmars.2021.627722.

Ip, Y.K., Ching, B., Hiong, K.C., Choo, C.Y.L., Boo, M.V., Wong, W.P., Chew, S.F., 2015. Light induces changes in activities of Na^+/K^+-ATPase, H^+/K^+-ATPase and glutamine synthetase in tissues involved directly or indirectly in light-enhanced calcification in the giant clam, *Tridacna squamosa*. Front. Physiol. 6. https://doi.org/10.3389/fphys.2015.00068.

Ip, Y.K., Hiong, K.C., Goh, E.J.K., Boo, M.V., Choo, C.Y.L., Ching, B., Wong, W.P., Chew, S.F., 2017. The whitish inner mantle of the giant clam, *Tridacna squamosa*, expresses an Apical Plasma Membrane Ca^{2+}-ATPase (PMCA) which displays light-dependent gene and protein expressions. Front. Physiol. 8, 781. https://doi.org/10.3389/fphys.2017.00781.

Jantzen, C., Wild, C., El-Zibdah, M., Roa-Quiaoit, H.A., Haacke, C., Richter, C., 2008. Photosynthetic performance of giant clams, *Tridacna maxima* and *T. squamosa*. Red Sea. Mar Biol 155, 211–221. https://doi.org/10.1007/s00227-008-1019-7.

Johnson, G.C., Karajah, M.T., Mayo, K., Armenta, T.C., Blumstein, D.T., 2017. The bigger they are the better they taste: size predicts predation risk and anti-predator behavior in giant clams. J. Zool. 301, 102–107. https://doi.org/10.1111/jzo.12401.

Jolivet, A., Asplin, L., Strand, Ø., Thébault, J., Chauvaud, L., 2015. Coastal upwelling in Norway recorded in Great Scallop shells. Limnol. Oceanogr. 60, 1265–1275. https://doi.org/10.1002/lno.10093.

Jones, D.S., 1980. Annual cycle of shell growth increment formation in two continental shelf bivalves and its paleoecologic significance. Paleobiology 6, 331–340. https://doi.org/10.1017/S0094837300006837.

Jones, D.S., 1981. Annual growth increments in shells of *Spisula solidissima* record marine temperature variability. Science 211, 165–167. https://doi.org/10.1126/science.211.4478.165.

Karperien, A., 2013. FracLac for ImageJ. NIH. https://doi.org/10.13140/2.1.4775.8402.

Killam, D., Das, S., Martindale, R.C., Gray, K.E., Paytan, A., Junium, C.K., 2023a. Photosymbiosis and nutrient utilization in giant clams revealed by nitrogen isotope sclerochronology. Geochim. Cosmochim. Acta 359, 165–175. https://doi.org/10.1016/j.gca.2023.08.018.

Killam, D., Thompson, D., Morgan, K., Russell, M., 2023b. Giant clams as open-source, scalable reef environmental biomonitors. PLoS One 18, e0278752. https://doi.org/10.1371/journal.pone.0278752.

Klumpp, D., Griffiths, C., 1994. Contributions of phototrophic and heterotrophic nutrition to the metabolic and growth requirements of four species of giant clam (Tridacnidae). Mar. Ecol. Prog. Ser. 115, 103–115. https://doi.org/10.3354/meps115103.

Klumpp, D.W., Lucas, J.S., 1994. Nutritional ecology of the giant clams *Tridacna tevoroa* and *T. derasa* from Tonga: influence of light on filter-feeding and photosynthesis. Mar. Ecol. Prog. Ser. 107, 147–156.

Lazareth, C.E., Le Cornec, F., Candaudap, F., Freydier, R., 2013. Trace element heterogeneity along isochronous growth layers in bivalve shell: consequences for environmental reconstruction. Palaeogeogr. Palaeoclimatol. Palaeoecol. 373, 39–49. https://doi.org/10.1016/j.palaeo.2011.04.024.

Legland, D., Arganda-Carreras, I., Andrey, P., 2016. MorphoLibJ: integrated library and plugins for mathematical morphology with ImageJ. Bioinformatics 32, 3532–3534. https://doi.org/10.1093/bioinformatics/btw413.

Liu, C., Yan, H., Wang, G., Zhao, L., Hu, Y., Zhou, P., Luo, F., Yang, H., Dodson, J., 2021. Species specific Sr/Ca-$\delta^{18}O$ relationships for three Tridacnidae species from the northern South China Sea. Chem. Geol. 584, 120519. https://doi.org/10.1016/j.chemgeo.2021.120519.

Liu, C., Zhao, L., Zhao, N., Yang, W., Hao, J., Qu, X., Liu, S., Dodson, J., Yan, H., 2022. Novel methods of resolving daily growth patterns in giant clam (*Tridacna* spp.) shells. Ecol. Indic. 134, 108480. https://doi.org/10.1016/j.ecolind.2021.108480.

Liu, C., Yan, H., Zhao, L., Zhao, N., Luo, F., Wen, H., Yang, H., Yang, W., Hao, J., Liang, C., Tanaka, K., Murakami-Sugihara, N., Shirai, K., Takahata, N., Dodson, J., Schöne, B.R., 2024. Potential environment effect on ultrahigh resolution Sr/Ca of giant clam shells from South China Sea. Coral Reefs 43, 1511–1521. https://doi.org/10.1007/s00338-024-02555-z.

Lorens, R.B., Bender, M.L., 1977. Physiological exclusion of magnesium from *Mytilus edulis* calcite. Nature 269, 793–794. https://doi.org/10.1038/269793a0.

Lucas, J.S., Nash, W.J., Crawford, C.M., Braley, R.D., 1989. Environmental influences on growth and survival during the ocean-nursery rearing of giant clams, *Tridacna gigas* (L.). Aquaculture 80, 45–61. https://doi.org/10.1016/0044-8486(89)90272-X.

Marchitto, T.M., Jones, G.A., Goodfriend, G.A., Weidman, C.R., 2000. Precise temporal correlation of Holocene mollusk shells using sclerochronology. Quat. Res. 53, 236–246. https://doi.org/10.1006/qres.1999.2107.

Menadakis, M., Maroulis, G., Koutsoukos, P.G., 2008. Incorporation of Mg^{2+}, Sr^{2+}, Ba^{2+} and Zn^{2+} into aragonite and comparison with calcite. J. Math. Chem. 46, 484–491. https://doi.org/10.1007/s10910-008-9490-4.

Mills, K., Muir, D.D., Oldroyd, A., John, E.H., Santodomingo, N., Johnson, K.G., Hussein, M.A.S., Sosdian, S., 2024a. Microstructure and crystallographic texture data in modern giant clam shells (*Tridacna squamosa* and *Hippopus hippopus*). Data Brief 52, 109947. https://doi.org/10.1016/j.dib.2023.109947.

Mills, K., Sosdian, S., Muir, D., John, E., Nadia, S., Johnson, K., Buse, B., Waheed, Z., 2024b. Giant clams modify crystallographic and geochemical pathways of shell formation in response to turbidity (preprint). In Review. https://doi.org/10.21203/rs.3.rs-3832703/v1.

Mook, W.G., Vogel, J.C., 1968. Isotopic equilibrium between shells and their environment. Science 159, 874–875. https://doi.org/10.1126/science.159.3817.874.

Pang, C.Z., Boo, M.V., Ip, Y.K., Chew, S.F., 2022. Symbiotic dinoflagellates of the giant clam, *Tridacna squamosa*, express Ammonium Transporter 2 at the plasma membrane and increase its expression levels during illumination. Front. Mar. Sci. 9, 835574. https://doi.org/10.3389/fmars.2022.835574.

Pätzold, J., Heinrichs, J.P., Wolschendorf, K., Wefer, G., 1991. Correlation of stable oxygen isotope temperature record with light attenuation profiles in reef-dwelling *Tridacna* shells. Coral Reefs 10, 65–69. https://doi.org/10.1007/BF00571825.

Peharda, M., Schöne, B.R., Black, B.A., Corrège, T., 2021. Advances of sclerochronology research in the last decade. Palaeogeogr. Palaeoclimatol. Palaeoecol. 570, 110371. https://doi.org/10.1016/j.palaeo.2021.110371.

Piwoni-Piórewicz, A., Strekopytov, S., Humphreys-Williams, E., Kukliński, P., 2021. The patterns of elemental concentration (Ca, Na, Sr, Mg, Mn, Ba, Cu, Pb, V, Y, U and Cd) in shells of invertebrates representing different $CaCO_3$ polymorphs: a case study from the brackish Gulf of Gdańsk (the Baltic Sea). Biogeosciences 18, 707–728. https://doi.org/10.5194/bg-18-707-2021.

Reynolds, D.J., Scourse, J.D., Halloran, P.R., Nederbragt, A.J., Wanamaker, A.D., Butler, P.G., Richardson, C.A., Heinemeier, J., Eiríksson, J., Knudsen, K.L., Hall, I.R., 2016. Annually resolved North Atlantic marine climate over the last millennium. Nat. Commun. 7, 13502. https://doi.org/10.1038/ncomms13502.

Rosewater, J., 1965. The Family Tridacnidae in the Indo-Pacific. Department of Mollusks, Academy of Natural Sciences of Philadelphia.

Sano, Y., Kobayashi, S., Shirai, K., Takahata, N., Matsumoto, K., Watanabe, T., Sowa, K., Iwai, K., 2012. Past daily light cycle recorded in the strontium/calcium ratios of giant clam shells. Nat. Commun. 3, 761. https://doi.org/10.1038/ncomms1763.

Schindelin, J., Arganda-Carreras, I., Frise, E., Kaynig, V., Longair, M., Pietzsch, T., Preibisch, S., Rueden, C., Saalfeld, S., Schmid, B., Tinevez, J.-Y., White, D.J., Hartenstein, V., Eliceiri, K., Tomancak, P., Cardona, A., 2012. Fiji: an open-source platform for biological-image analysis. Nat. Methods 9, 676–682. https://doi.org/10.1038/nmeth.2019.

Schöne, B.R., Fiebig, J., Pfeiffer, M., Gleβ, R., Hickson, J., Johnson, A.L.A., Dreyer, W., Oschmann, W., 2005. Climate records from a bivalved Methuselah (*Arctica islandica*, Mollusca; Iceland). Palaeogeogr. Palaeoclimatol. Palaeoecol. 228, 130–148. https://doi.org/10.1016/j.palaeo.2005.03.049.

Schöne, B.R., Zhang, Z., Radermacher, P., Thébault, J., Jacob, D.E., Nunn, E.V., Maurer, A.-F., 2011. Sr/Ca and Mg/Ca ratios of ontogenetically old, long-lived bivalve shells (*Arctica islandica*) and their function as paleotemperature proxies. Palaeogeogr. Palaeoclimatol. Palaeoecol. 302, 52–64. https://doi.org/10.1016/j.palaeo.2010.03.016.

Schöne, B.R., Radermacher, P., Zhang, Z., Jacob, D.E., 2013. Crystal fabrics and element impurities (Sr/Ca, Mg/Ca, and Ba/Ca) in shells of *Arctica islandica* – Implications for paleoclimate reconstructions. Palaeogeogr. Palaeoclimatol. Palaeoecol. 373, 50–59. https://doi.org/10.1016/j.palaeo.2011.05.013.

Schöne, B.R., Meret, A.E., Baier, S.M., Fiebig, J., Esper, J., McDonnell, J., Pfister, L., 2020. Freshwater pearl mussels from northern Sweden serve as long-term, high-resolution stream water isotope recorders. Hydrol. Earth Syst. Sci. 24, 673–696. https://doi.org/10.5194/hess-24-673-2020.

Shannon, R.D., 1976. Revised effective ionic radii and systematic studies of interatomic distances in halides and chalcogenides. Acta Cryst A 32, 751–767. https://doi.org/10.1107/S0567739476001551.

Shirai, K., Schöne, B.R., Miyaji, T., Radarmacher, P., Krause, R.A., Tanabe, K., 2014. Assessment of the mechanism of elemental incorporation into bivalve shells (*Arctica islandica*) based on elemental distribution at the microstructural scale. Geochim. Cosmochim. Acta 126, 307–320. https://doi.org/10.1016/j.gca.2013.10.050.

Sun, Y., Sun, M., Wei, G., Lee, T., Nie, B., Yu, Z., 2004. Strontium contents of a Porites coral from Xisha Island, South China Sea: a proxy for sea-surface temperature of the 20th century. Paleoceanography 19. https://doi.org/10.1029/2003PA000959.

Tanabe, K., Mimura, T., Miyaji, T., Shirai, K., Kubota, K., Murakami-Sugihara, N., Schöne, B.R., 2017. Interannual to decadal variability of summer sea surface temperature in the Sea of Okhotsk recorded in the shell growth history of Stimpson's hard clams (*Mercenaria stimpsoni*). Glob. Planet. Chang. 157, 35–47. https://doi.org/10.1016/j.gloplacha.2017.08.010.

Teh, L.S.X., Poo, J.S.T., Boo, M.V., Chew, S.F., Ip, Y.K., 2021. Using glutamine synthetase 1 to evaluate the symbionts' potential of ammonia assimilation and their responses to illumination in five organs of the giant clam, *Tridacna squamosa*. Comp. Biochem. Physiol. A Mol. Integr. Physiol. 255, 110914. https://doi.org/10.1016/j.cbpa.2021.110914.

Van Wynsberge, S., Andréfouët, S., Gaertner-Mazouni, N., Wabnitz, C.C.C., Menoud, M., Le Moullac, G., Levy, P., Gilbert, A., Remoissenet, G., 2017. Growth, survival and reproduction of the giant clam *Tridacna maxima* (Röding 1798, Bivalvia) in two contrasting lagoons in French Polynesia. PLoS One 12, e0170565. https://doi.org/10.1371/journal.pone.0170565.

Waisman, A., Norris, A.M., Elías Costa, M., Kopinke, D., 2021. Automatic and unbiased segmentation and quantification of myofibers in skeletal muscle. Sci. Rep. 11, 11793. https://doi.org/10.1038/s41598-021-91191-6.

Wanamaker, A.D., Kreutz, K.J., Wilson, T., Borns Jr., H.W., Introne, D.S., Feindel, S., 2008. Experimentally determined Mg/ca and Sr/Ca ratios in juvenile bivalve calcite for *Mytilus edulis*: implications for paleotemperature reconstructions. Geo-Mar. Lett. 28, 359–368. https://doi.org/10.1007/s00367-008-0112-8.

Warter, V., Müller, W., 2017. Daily growth and tidal rhythms in Miocene and modern giant clams revealed via ultra-high resolution LA-ICPMS analysis – a novel methodological approach towards improved sclerochemistry. Palaeogeogr. Palaeoclimatol. Palaeoecol. 465, 362–375. https://doi.org/10.1016/j.palaeo.2016.03.019. New research in the methods and applications of sclerochronology.

Warter, V., Erez, J., Müller, W., 2018. Environmental and physiological controls on daily trace element incorporation in *Tridacna crocea* from combined laboratory culturing and ultra-high resolution LA-ICP-MS analysis. Palaeogeogr. Palaeoclimatol. Palaeoecol. 496, 32–47. https://doi.org/10.1016/j.palaeo.2017.12.038.

Watanabe, T., Oba, T., 1999. Daily reconstruction of water temperature from oxygen isotopic ratios of a modern *Tridacna* shell using a freezing microtome sampling technique. J. Geophys. Res. 104, 20667–20674. https://doi.org/10.1029/1999JC900097.

Watson, E.B., 1996. Surface enrichment and trace-element uptake during crystal growth. Geochim. Cosmochim. Acta 60, 5013–5020. https://doi.org/10.1016/S0016-7037(96)00299-2.

Watson, E.B., 2004. A conceptual model for near-surface kinetic controls on the trace-element and stable isotope composition of abiogenic calcite crystals. Geochim. Cosmochim. Acta 68, 1473–1488. https://doi.org/10.1016/j.gca.2003.10.003.

Weidman, C.R., Jones, G.A., Kyger, 1994. The long-lived mollusc *Arctica islandica*: a new paleoceanographic tool for the reconstruction of bottom temperatures for the continental shelves of the northern North Atlantic Ocean. J. Geophys. Res. 99, 18305–18314. https://doi.org/10.1029/94JC01882.

Yan, H., 2020. Daily growth bands of giant clam shell: a potential paleoweather recorder. Solid Earth Sci. 5, 249–253. https://doi.org/10.1016/j.sesci.2020.10.001.

Yan, H., Shao, D., Wang, Y., Sun, L., 2011. High resolution Sr/Ca profile of *Tridacna gigas* from Xisha Islands of South China Sea and its potential application on sea surface temperature reconstruction. J. Earth Environ. 381–386 (In Chinese with English abstract).

Yan, H., Shao, D., Wang, Y., Sun, L., 2013. Sr/Ca profile of long-lived *Tridacna gigas* bivalves from South China Sea: a new high-resolution SST proxy. Geochim. Cosmochim. Acta 112, 52–65. https://doi.org/10.1016/j.gca.2013.03.007.

Yan, H., Shao, D., Wang, Y., Sun, L., 2014. Sr/Ca differences within and among three Tridacnidae species from the South China Sea: implication for paleoclimate reconstruction. Chem. Geol. 390, 22–31. https://doi.org/10.1016/j.chemgeo.2014.10.011.

Yan, H., Sun, L., Shao, D., Wang, Y., 2015. Seawater temperature seasonality in the South China Sea during the late Holocene derived from high-resolution Sr/Ca ratios of *Tridacna gigas*. Quat. Res. 83, 298–306. https://doi.org/10.1016/j.yqres.2014.12.001.

Yan, H., Liu, C., An, Z., Yang, W., Yang, Yuanjian, Huang, P., Qiu, S., Zhou, P., Zhao, N., Fei, H., Ma, X., Shi, G., Dodson, J., Hao, J., Yu, K., Wei, G., Yang, Yanan, Jin, Z., Zhou, W., 2020. Extreme weather events recorded by daily to hourly resolution biogeochemical proxies of marine giant clam shells. Proc. Natl. Acad. Sci. U. S. A. 117, 7038–7043. https://doi.org/10.1073/pnas.1916784117.

Yan, H., Zhao, N., Zhou, P., Liu, C., Fei, H., Li, M., Liu, F., Yang, Y., Yang, W., Dodson, J., 2021. The first detection of the Madden-Julian Oscillation signal in daily to hourly resolution proxy records derived from a natural archive of giant clam shell (*Tridacna* spp.). Earth Planet. Sci. Lett. 555, 116703. https://doi.org/10.1016/j.epsl.2020.116703.